Alma Mater Studiorum Università di Bologna
Archivio istituzionale della ricerca

Material model robust identification procedure from dynamical measurements made on a flexible specimen-frame system

20 February 2025

Material model robust identification procedure from dynamical measurements made on a flexible specimen-frame system.

Authors and Affiliations:

Stefano Amadori*,[a] , Giuseppe Catania[b]

[a]Ciri-Mam, University of Bologna, Viale Risorgimento 2, 40136 Bologna (BO), Italy, email: stefano.amadori4@unibo.it

[b]Ciri-Mam, DIN, Department of Industrial Engineering, University of Bologna, Viale Risorgimento 2, 40136 Bologna (BO), Italy, email: giuseppe.catania@unibo.it

Abstract:

A procedure for the identification of the material model of beam specimens by means of harmonic force and displacement measurements in flexural condition is presented. Input-output frequency response function (FRF) evaluations are used in standard DMA instruments to estimate the material stress-strain frequency response function. Nevertheless, the contribution of the instrument frame model coupling and of the inertial contribution of the excitation moving substructure to the input-output FRFs can make such estimates meaningless in most practical applications, especially if a wide excitation frequency range is taken into account. In this work the instrument frame model contribution is estimated by means of doing calibration measurements on some reference beams and processing them by a procedure based on optimization algorithms. A signal processing-based procedure is also proposed to identify the optimal frame model rational function fit by eliminating computational and noise related contribution. The identified rational frame model is used to obtain the material model in the frequency domain being filtered from the contribution of the experimental system. The proposed technique robustness is tested on some numerical model cases. The same technique is then applied to some dynamical measurements made on specimens of different materials. The results are shown and critically discussed.

*Corresponding author: Stefano Amadori
e-mail: stefano.amadori4@unibo.it

Keywords:

1.Introduction

Dynamic Mechanical Analysis (DMA) test instruments are commonly employed to investigate the mechanical behaviour of materials at different temperatures and frequencies [1-4]. They can be used to identify the constitutive models of tested specimen in the frequency domain [5,6], and can also be employed to validate material models by means of measurements in different, instrument dependent, frequency ranges [4]. In a typical dynamic measurement context, a time varying excitation is applied and measured, by means of a mobile measuring subsystem, to an experimental degree of freedom (dof) of a specimen of known geometry and the displacement response is obtained and measured in the same dof as well. Commercially available DMA instruments are designed to work at different frequency ranges, the maximum frequency value being limited by the instrument structural frequency dependent receptance, and many experimental configurations can be employed to test specimens of different geometries [1-4,7,8]. Simple specimens, for example beams that can be described by a known beam model, are tested and the experimental boundary condition are made to be as close as possible to the standard boundary conditions assumed in the reference beam model [3,9]. Nevertheless, theoretical standard beam end conditions are generally very far from real boundary conditions related to such context. To account for that contribution, known commercial test applications apply a calibration procedure to identify the static elastic stiffness modelling the ideal coupling between a rigid frame and the beam specimen and to also identify the lumped mass associated to the mobile measuring subsystem. A simple, but generally non consistent and non-effective lumped parameter frame model approach results. Literature reports that such simple models generally lead to unsatisfying results [9-11] as they fail to accurately describe the specimen under study dynamic behaviour in the medium and high measurement frequency range [7,11].
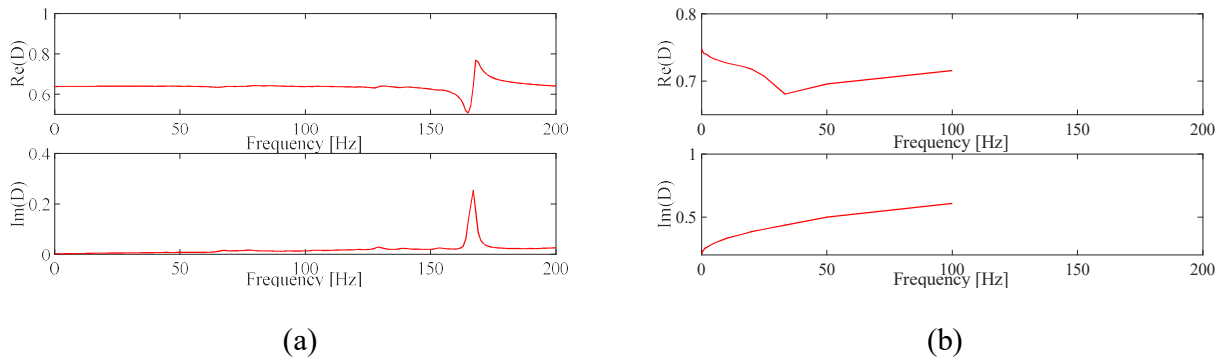
Fig.1: DMA experimental results for: (a) beam B1 (measuring system I1) and (b) B2 (measuring system I2, right).

As a matter of example, Fig.1 shows some experimental results concerning the $D(j \cdot \omega)$ σ stress versus ε strain model identification of homogeneous C67 harmonic steel made by means of different beam specimens and also different DMA test systems. Two beams (B1, B2), measured by means of two different instruments (I1. I2), are shown in Fig.1, with B1 (tested with I1) having length 17.5 mm, width 12.8 mm, thickness 0.75 mm, and B2 (tested with I2) having length 16 mm, width 2.97 mm, thickness 0.5 mm. For both the specimens, the same experimental condition set-up was adopted, i.e. clamped double pendulum boundary conditions, constant vibration amplitude $v = 10$ μm at the mobile end of the beam ($\varepsilon_{max} < 1.5 \cdot 10^{-4}$), the measured frequency range was [0.1-200] Hz for I1, [0.1-100] Hz for I2. The standard calibration procedure associated to each instrument is used to estimate $D(j \cdot \omega)$.

Since low strain and ambient temperature experimental conditions are considered, the results shown in Fig.1 are unsatisfying if compared with the expected reference Hooke model behaviour, i.e. $D(j \cdot \omega) = 1$.

More effective calibration and identification techniques are needed to obtain more accurate results, and an innovative procedure is proposed in this work.

To obtain an accurate structural model of the instrument frame to be coupled with the specimen beam model and to define a procedure being able to filter the estimated FRFs from the frame coupling effective boundary conditions, typically a multi degree of freedom (mdof) experimental inverse modelling approach is required, and many effective techniques are known [12-14]. Such techniques typically make use of a secondary test measurement system, including accelerometer, laser doppler vibrometer sensors, impulse and shaker excitation systems and a multi-channel data acquisition system

as well [13,15,16], since such tools are not directly available from within the typical DMA instrument. The adoption of mdof experimental identification techniques can significantly improve the system calibration accuracy, but the resulting calibration procedure, to be adopted before any new measurement campaign is started, is not generally compatible with the standard experimental practice, and to the expected value of the costs.

The calibration technique proposed in this work takes into account of the real specimen boundary conditions, of the inertial effect of the mobile measuring subsystem, and differs from the known approaches [12-17] since only the single experimental dof input-output data obtained from a single experimental dof DMA system are employed to identify a multi-dof test system and a procedure is also applied to eliminate any computational and noise related contribution to the estimated specimen and frame rational model.

Known material identification techniques made it possible to obtain the $D(j \cdot \omega)$ material σ stress versus ε strain relationship:

$$\sigma(j \cdot \omega) = E(j \cdot \omega) \cdot \varepsilon(j \cdot \omega) = E_0 \cdot D(j \cdot \omega) \cdot \varepsilon(j \cdot \omega) \tag{1}$$

by processing the instrument output and taking into account of the assumed beam specimen model, i.e. Timoshenko or Euler-Bernoulli model [18], with clamped-sliding boundary conditions. The beam inertial action contribution in the measured frequency range $\boldsymbol{\omega} = \{\omega_1 \quad \ldots \quad \omega_f \ldots \omega_N\}$ can also be taken into account [4] in the measurement processing procedure.

It must be noted that $E_0 \cdot D(j \cdot \omega)$ can be modelled by means of an n_k order generalized Kelvin model [19], i.e. n_k Kelvin blocks connected in series, where a single Kelvin block is a parallel connection of an elastic Hooke (E_i) and a viscous Newton (β_i) block unit. For the i-th block Eq.(1) holds:

$$\tilde{\sigma} = (E_i + j \cdot \omega \cdot \beta_i) \cdot \tilde{\varepsilon}_i \quad , \quad i = 1, \ldots, n_K \tag{2}$$

where $(\tilde{\ })$ is the Fourier transform operator. Since $\tilde{\varepsilon} = \tilde{\varepsilon}_i + \ldots + \tilde{\varepsilon}_i + \ldots + \tilde{\varepsilon}_{n_K}$, from Eq,(2) [19]:

$$D(j \cdot \omega) = \frac{b_{n_K} \cdot (j \cdot \omega)^{n_K} + \ldots + b_\ell \cdot (j \cdot \omega) + 1}{a_{n_K - 1} \cdot (j \cdot \omega)^{n_K - 1} + \ldots + a_1 \cdot (j \cdot \omega) + 1}; \quad E_0 = \left(\sum_{i=1}^{n_K} \frac{1}{E_i}\right)^{-1}; \quad a_i, b_\ell \in \Re \sqrt{b^2 - 4ac} \tag{3}$$

In Eq. (3) the constant E_0 is the material modulus at $\omega = 0$ and its value can be estimated from static measurements or extrapolated from dynamical measurement estimates as the frequency goes to zero.

In these authors previous work [4] a rational function fit approach based on monomials and orthogonal Forsythe polynomial bases was considered to obtain a $D(j \cdot \omega)$ rational fit but the instrument frame contribution was not taken into account. In the novel modelling approach proposed in this work, a 2-dofs, multi-pole instrument frame model in the frequency domain is first identified by means of measurements made on different known specimens. A new procedure for the identification of the rational model real parameters of the instrument frame frequency transfer function is proposed in this work, making it possible to discard computational terms. This rational fit procedure is generalized to employ different polynomial bases, i.e. monomial, Forsythe, Chebyshev and Legendre polynomials, and is based on the least square minimum approach [17,20-23]. The instrument frame model is used to obtain a $D(j \cdot \omega)$ estimate from within experimental measurement on a test specimen by means of an optimisation-based algorithm, and a $D(j \cdot \omega)$ physically sound rational model can then be obtained by means of the same procedure employed to identify the rational instrument frame model. The robustness of this calibration procedure is tested by means of numerical model test cases with added noise and then is applied to experimental measurements and validated as well. The proposed identification procedures and the results are critically discussed at the end of this paper.

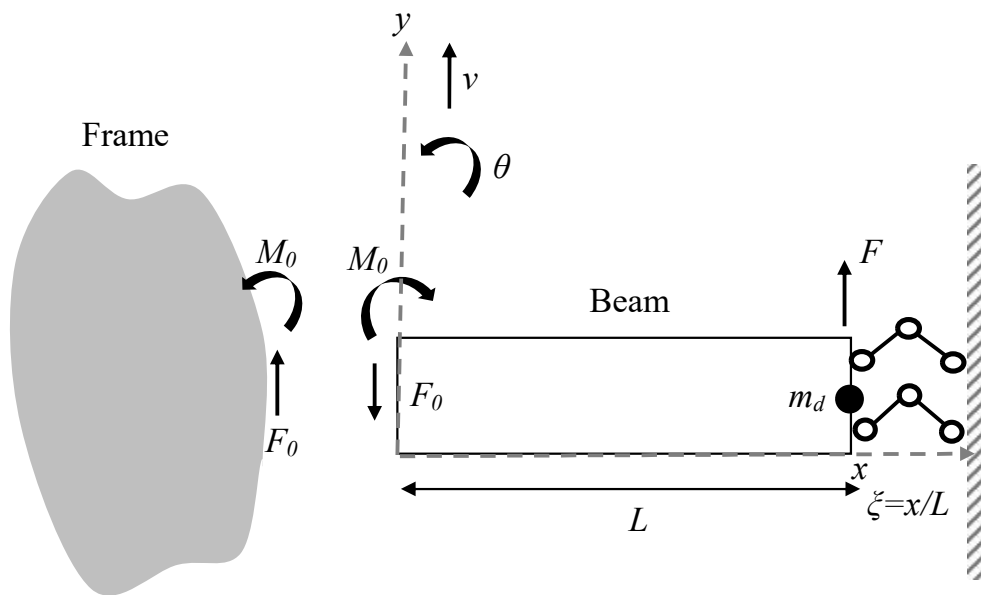## 2. Experimental setup and model assumptions

Fig.2: Experimental setup.

A schematic representation of a typical standard measurement system experimental set-up is shown in Fig.2, showing a single-cantilever standard mounting configuration of the beam specimen made of the material under test [1-4,7]. The system is composed of the instrument frame, the beam specimen and the mobile excitation-measuring subsystem (modelled by means of a lumped mass m_d) at the mobile end of the beam. Specimens in the form of slender, uniform, homogeneous beams are excited by means of a sinusoidal flexural force at different frequencies at the mobile beam end, where both excitation and displacement response are synchronously measured at the same experimental degree of freedom model (Fig.2). Clamped-sliding beam boundary conditions can be assumed for the test specimen, but ideal, rigid frame exhibiting null displacement under external excitation should be assumed as well. Taking into account of frame continuously distributed elastic and inertial properties, in this approach beam free-sliding boundary conditions are assumed instead (Fig.2), and the beam free end vertical displacement and rotation are assumed to coincide with 2 frame experimental dofs, these two dofs coinciding with v displacement and θ rotation of the instrument frame and of the specimen fixed end. The kinematical coupling between beam and frame dofs, in the frequency domain, is defined by the unknown, to be identified, frame response function, being generally complex, frequency dependent, and exhibiting a generally unknown number of system poles. The m_d inertial mass is lumped in the sliding end.

To take into account of the frame dynamic contribution, flexural excitation force-displacement measurements are made on a set of uniform beam specimens made of a reference material and the known mechanical data related to the specimens are processed by means of an optimisation algorithm to identify a 2 dofs-multiple poles frame system model, the two physical dofs coinciding with v displacement and θ rotation of the instrument frame coupled with the specimen fixed end.

It must be observed that the instrument frame frequency transfer function matrix resulting from the identified system model can be associated to a classical second order, 2 dofs, n_p poles, mechanical system, where the matrix elements can be modelled by means of the ratio of a $n_p - 1$ degree $p_{n_p-1}(j \cdot \omega)$ polynomial function to a n_p degree $p_{n_p}(j \cdot \omega)$ polynomial function, where real valued polynomial coefficients are assumed.

The beam specimen is modelled by means of the Euler-Bernoulli beam theory [9,18], since slender beam test specimens are taken into account here. A kinematical small displacement and deformation

field is assumed, and the beam transverse displacement $v(\xi,t)$ continuous state variable (Fig.2) is assumed. A spectral approach is considered [24]. The transverse displacement v kinematical variable is approximated by means of the product of two separate functions of the normalized ξ coordinate and of the time t:

$$v \cong \mathbf{\Psi}(\xi) \cdot \mathbf{\delta}(t) \tag{4}$$

where $\mathbf{\delta}(t)$ refers to the unknown beam dofs and $\mathbf{\Psi}(\xi)$ is made up of n normalized, orthogonal, known eigenfunctions, satisfying the free-sliding beam boundary conditions [4,18]:

$$\mathbf{\Psi}(\xi) = \{\Psi_1(\xi) \quad \dots \quad \Psi_n(\xi)\} \ , \quad \Psi_i(\xi) = \cosh z_i \cdot \xi + \cos z_i \cdot \xi + Q_i \cdot (\sinh z_i \cdot \xi + \sin z_i \cdot \xi); \ Q_i = -\tanh z_i \tag{5}$$

and z_i are the infinite solutions of the equation $\tan z_i + \tanh z_i = 0$, $z_i \cong (4 \cdot i - 1) \cdot \dfrac{\pi}{4}$. As shown in

Fig.2, test force F is applied at the sliding end of the beam ($\xi = 1$), force F_0 and momentum M_0 reactions result at the free end of the beam ($\xi = 0$), and F_0, M_0 reactions result at the coupled frame dofs as well. The inertial contribution of the m_d lumped mass at the sliding beam end is also taken into account. Since homogeneous, uniform beam assumptions are made, the following beam differential equations of motion can be obtained by imposing the beam total potential energy stationarity condition to an arbitrary beam infinitesimal element associated to ξ position, $d\xi$ length, where beam boundary conditions are satisfied from Eq.(5) assumptions:

$$\frac{E_0 \cdot D(j \cdot \omega) \cdot I}{L^3} \cdot diag(\mathbf{z}^4) \cdot \mathbf{\delta} + L \cdot \rho \cdot A \cdot \left(\mathbf{I} + \frac{m_d}{L \cdot \rho \cdot A} \cdot \mathbf{\Psi}^T(1) \cdot \mathbf{\Psi}(1) \right) \cdot \ddot{\mathbf{\delta}} + \mathbf{\Psi}^T(0) \cdot F_0 + \frac{\mathbf{\Psi}'^T(0)}{L} \cdot M_0 - \mathbf{\Psi}^T(1) \cdot F = \mathbf{0}$$

$$\left(\int_0^1 \mathbf{\Psi}^T(\xi) \cdot \mathbf{\Psi}(\xi) \cdot d\xi \right) = \mathbf{I} \ , \quad \left(\int_0^1 \mathbf{\Psi}''^T(\xi) \cdot \mathbf{\Psi}''(\xi) \cdot d\xi \right) = diag(\mathbf{z}^4) \ , \quad \mathbf{z} = \{z_1 \quad \dots \quad z_n\} \ . \tag{6}$$

In Eq.(6), $(\ )^T$ is the transpose operator, $(\ )' = \partial(\ )/\partial \xi = L \cdot \partial(\ )/\partial x$, $(\dot{\ }) = \partial(\ )/\partial t$, I is the beam transverse section moment, A is the beam section area and ρ the material density. Applying to Eq.(4) the Fourier transform operator:

$$\tilde{v} = \mathbf{\Psi}(\xi) \cdot \mathbf{\Delta}(j \cdot \omega)$$

$$\tilde{\theta} = \frac{1}{L} \cdot \mathbf{\Psi}'(\xi) \cdot \mathbf{\Delta}(j \cdot \omega) \tag{7}$$

By Fourier transforming Eq.(6), the following result can be obtained:

$$\Delta(j\cdot\omega)=\left\{\begin{array}{c}\Delta_1\\ \vdots\\ \Delta_n\end{array}\right\}=$$

$$=\left[\frac{E_0\cdot D(j\cdot\omega)\cdot I}{L^3}\cdot diag\left(\mathbf{z}^4\right)-\omega^2\cdot L\cdot\rho\cdot A\cdot\left(\mathbf{I}+\frac{m_d}{L\cdot\rho\cdot A}\cdot\mathbf{\Psi}^T(1)\cdot\mathbf{\Psi}(1)\right)\right]^{-1}\cdot\left[\mathbf{\Psi}^T(0)\quad\frac{\mathbf{\Psi}'^T(0)}{L}\quad\mathbf{\Psi}^T(1)\right]\cdot\mathbf{F}(j\cdot\omega),\qquad(8)$$

$$\mathbf{F}(j\cdot\omega)=\left\{-\tilde{F}_0(j\cdot\omega)\quad-\tilde{M}_0(j\cdot\omega)\quad\tilde{F}(j\cdot\omega)\right\}^T$$

Since:

$$\left\{\begin{array}{c}\tilde{v}(0,j\cdot\omega)\\ \tilde{\theta}(0,j\cdot\omega)\\ \tilde{v}(1,j\cdot\omega)\end{array}\right\}=\left[\begin{array}{c}\mathbf{\Psi}(0)\\ \frac{1}{L}\mathbf{\Psi}'(0)\\ \mathbf{\Psi}(1)\end{array}\right]\cdot\Delta(\omega)=\left[\begin{array}{c}\mathbf{\Psi}(0)\\ \frac{1}{L}\mathbf{\Psi}'(0)\\ \mathbf{\Psi}(1)\end{array}\right]\cdot\left\{\begin{array}{c}\Delta_1(j\cdot\omega)\\ \dots\\ \Delta_n(j\cdot\omega)\end{array}\right\}\qquad(9)$$

From Eqs.(8-9):

$$\left\{\begin{array}{c}\tilde{v}(0,j\cdot\omega)\\ \tilde{\theta}(0,j\cdot\omega)\\ \tilde{v}(1,j\cdot\omega)\end{array}\right\}=\mathbf{\Gamma}\cdot\mathbf{F}=\left[\begin{array}{ccc}\Gamma_{11}(j\cdot\omega)&\Gamma_{12}(j\cdot\omega)&\Gamma_{13}(j\cdot\omega)\\ \Gamma_{21}(j\cdot\omega)&\Gamma_{22}(j\cdot\omega)&\Gamma_{23}(j\cdot\omega)\\ \Gamma_{31}(j\cdot\omega)&\Gamma_{32}(j\cdot\omega)&\Gamma_{33}(j\cdot\omega)\end{array}\right]\cdot\left\{\begin{array}{c}-\tilde{F}_0(j\cdot\omega)\\ -\tilde{M}_0(j\cdot\omega)\\ \tilde{F}(j\cdot\omega)\end{array}\right\},\qquad(10)$$

where:

$$\mathbf{\Gamma}(j\cdot\omega)=\left[\begin{array}{ccc}\sum_{k=1}^n\left(\Psi_k(0)\cdot\sum_{i=1}^n\Omega_{ki}\cdot\Psi_i(0)\right)&\frac{1}{L}\cdot\sum_{k=1}^n\left(\Psi_k(0)\cdot\sum_{i=1}^n\Omega_{ki}\cdot\Psi_i'(0)\right)&\sum_{k=1}^n\left(\Psi_k(0)\cdot\sum_{i=1}^n\Omega_{ki}\cdot\Psi_i(1)\right)\\ \frac{1}{L}\cdot\sum_{k=1}^n\left(\Psi_i'(0)\cdot\sum_{i=1}^n\Omega_{ki}\cdot\Psi_i(0)\right)&\frac{1}{L^2}\cdot\sum_{k=1}^n\left(\Psi_k'(0)\cdot\sum_{i=1}^n\Omega_{ki}\cdot\Psi_i'(0)\right)&\frac{1}{L}\cdot\sum_{k=1}^n\left(\Psi_i'(0)\cdot\sum_{i=1}^n\Omega_{ki}\cdot\Psi_i(1)\right)\\ \sum_{k=1}^n\left(\Psi_k(1)\cdot\sum_{i=1}^n\Omega_{ki}\cdot\Psi_i(0)\right)&\frac{1}{L}\cdot\sum_{k=1}^n\left(\Psi_k(1)\cdot\sum_{i=1}^n\Omega_{ki}\cdot\Psi_i'(0)\right)&\sum_{k=1}^n\left(\Psi_k(1)\cdot\sum_{i=1}^n\Omega_{ki}\cdot\Psi_i(1)\right)\end{array}\right],\qquad(11)$$

$$\mathbf{\Omega}(j\cdot\omega)=\left[\begin{array}{ccc}\Omega_{11}&\dots&\Omega_{1n}\\ \dots&\dots&\dots\\ \Omega_{n1}&\dots&\Omega_{nn}\end{array}\right]=\left[\frac{D(j\cdot\omega)\cdot I}{L^3}\cdot diag\left(\mathbf{z}^4\right)-\omega^2\cdot L\cdot\rho\cdot A\cdot\left(\mathbf{I}+\frac{m_d}{L\cdot\rho\cdot A}\cdot\mathbf{\Psi}^T(1)\cdot\mathbf{\Psi}(1)\right)\right]^{-1}.$$

The two dofs at the free end of the beam ($\tilde{v}(0,j\cdot\omega)$, $\tilde{\theta}(0,j\cdot\omega)$) are assumed to be congruent with the dofs associated to the instrument frame. The $\mathbf{X}(j\cdot\omega)$ frame frequency transfer function for $\tilde{v}(0,j\cdot\omega)$ and $\tilde{\theta}(0,j\cdot\omega)$ is assumed as:

$$\left\{\begin{array}{c}\tilde{v}(0,j\cdot\omega)\\ \tilde{\theta}(0,j\cdot\omega)\end{array}\right\}=\mathbf{X}(j\cdot\omega)\cdot\left\{\begin{array}{c}\tilde{F}_0\\ \tilde{M}_0\end{array}\right\}=\left[\begin{array}{cc}X_{11}(j\cdot\omega)&X_{12}(j\cdot\omega)\\ X_{12}(j\cdot\omega)&X_{22}(j\cdot\omega)\end{array}\right]\cdot\left\{\begin{array}{c}\tilde{F}_0\\ \tilde{M}_0\end{array}\right\}\qquad(12)$$

Combining Eqs.(10,12).

$$\begin{bmatrix} \Gamma_{11} & \Gamma_{12} \\ \Gamma_{21} & \Gamma_{22} \end{bmatrix} \cdot \begin{Bmatrix} -\tilde{F}_0 \\ -\tilde{M}_0 \end{Bmatrix} + \begin{Bmatrix} \Gamma_{13} \\ \Gamma_{23} \end{Bmatrix} \cdot \tilde{F} = \begin{bmatrix} X_{11} & X_{12} \\ X_{12} & X_{22} \end{bmatrix} \cdot \begin{Bmatrix} \tilde{F}_0 \\ \tilde{M}_0 \end{Bmatrix}$$

$$\tilde{v}(1, j \cdot \omega) = \Gamma_{33} \cdot \tilde{F} + \{ \Gamma_{31} \quad \Gamma_{32} \} \cdot \begin{Bmatrix} -\tilde{F}_0 \\ -\tilde{M}_0 \end{Bmatrix}$$

(13)

and from Eq.(13):

$$\begin{Bmatrix} \tilde{F}_0 \\ \tilde{M}_0 \end{Bmatrix} = \left(\begin{bmatrix} X_{11} & X_{12} \\ X_{12} & X_{22} \end{bmatrix} + \begin{bmatrix} \Gamma_{11} & \Gamma_{12} \\ \Gamma_{21} & \Gamma_{22} \end{bmatrix} \right)^{-1} \cdot \begin{Bmatrix} \Gamma_{13} \\ \Gamma_{23} \end{Bmatrix} \cdot \tilde{F}$$

$$\tilde{v}(1, j \cdot \omega) = \left(\Gamma_{33} - \{ \Gamma_{31} \quad \Gamma_{32} \} \cdot \left(\begin{bmatrix} X_{11} & X_{12} \\ X_{12} & X_{22} \end{bmatrix} + \begin{bmatrix} \Gamma_{11} & \Gamma_{12} \\ \Gamma_{21} & \Gamma_{22} \end{bmatrix} \right)^{-1} \cdot \begin{Bmatrix} \Gamma_{13} \\ \Gamma_{23} \end{Bmatrix} \right) \cdot \tilde{F}$$

(14)

In Eq.(14) the beam displacement at the sliding end, corresponding to the measurement data obtained from within a typical dynamic mechanical system, is explicitly expressed as a function of the unknown symmetric matrix $\mathbf{X}(j \cdot \omega)$. Frame model identification from the calibration procedure consists in identifying the independent $X_{11}(j \cdot \omega)$, $X_{12}(j \cdot \omega)$, $X_{22}(j \cdot \omega)$ frequency dependent terms, for every ω value from the experimental test measurement.

3 Instrument frame $\mathbf{X}(j \cdot \omega)$ model identification

A test setup of n_b reference beams with known geometry made of known material ($D(j \cdot \omega)$ is assumed to be known) are expected to be measured over a discrete frequency range $\boldsymbol{\omega} = \{ \omega_1 \quad \dots \quad \omega_f \ \dots \ \omega_N \}$. From Eq.(14) transfer function measurements only depend on the $\mathbf{X}(j \cdot \omega)$ unknown frame contribution matrix, since the specimen characteristics (geometry and material) are supposed to be known in advance. The m_d lumped mass model parameter associated to the measuring mobile model subsystem can be estimated by means of $\tilde{F}(j \cdot \omega_f)$ force and $\tilde{v}(j \cdot \omega_f)$ displacement measurements, made in the $\boldsymbol{\omega}$ frequency range, without a mounted specimen, i.e. only the mobile subsystem inertial excitation results:

$$m_d = \frac{1}{N} \cdot \sum_{f=1}^{N} \frac{1}{\omega_f^2} \cdot \left| \frac{\tilde{F}(j \cdot \omega_f)}{\tilde{v}(j \cdot \omega_f)} \right|$$

(15)

A set of n_b nonlinear equations in 3 unknowns with respect to ω_f frequency value results from a measuring $n_b \geq 3$ different beam specimens:

$$\begin{cases} H_f^1\left(\mathbf{X}(j\cdot\omega_f)\right)=HM_f^1 \\ \dots \\ H_f^{n_b}\left(\mathbf{X}(j\cdot\omega_f)\right)=HM_f^{n_b} \end{cases}, \quad f=1\dots N$$

$$\begin{cases} H_f^i\left(\mathbf{X}(j\cdot\omega_f)\right)=\Gamma_{33}^i-\left\{\Gamma_{31}^i \quad \Gamma_{32}^i\right\}\cdot\left(\mathbf{X}(j\cdot\omega_f)+\begin{bmatrix}\Gamma_{11}^i & \Gamma_{12}^i \\ \Gamma_{12}^i & \Gamma_{22}^i\end{bmatrix}\right)^{-1}\cdot\left\{\begin{matrix}\Gamma_{13}^i \\ \Gamma_{23}^i\end{matrix}\right\}, \\ HM_f^i=\left(\dfrac{\tilde{v}\left(1,j\cdot\omega_f\right)}{\tilde{F}\left(1,j\cdot\omega_f\right)}\right)_i \end{cases} \qquad (16)$$

and from Eq.(16):

$$\mathbf{H}_f=\left\{H_f^1 \quad \dots \quad H_f^{n_b}\right\}^T, \quad \mathbf{HM}_f=\left\{HM_f^1 \quad \dots \quad HM_f^{n_b}\right\}^T; \quad f=1,\dots,N \qquad (17).$$

A multi-step approach is proposed for $\mathbf{X}(j\cdot\omega)$ matrix identification.

Step1: for every ω_f frequency value the $\mathbf{e}_f$ error vector and Φ_f objective scalar function can be defined:

$$\begin{aligned} \mathbf{e}_f&=\mathbf{e}_f\left(\mathbf{X}(j\cdot\omega_f)\right)=\mathbf{H}_f\left(\mathbf{X}(j\cdot\omega_f)\right)-\mathbf{HM}_f \\ \Phi_f&=\Phi_f\left(\mathbf{X}(j\cdot\omega_f)\right)=\mathbf{e}_f^T\cdot\mathbf{e}_f \end{aligned}. \qquad (18)$$

A multi-step constrained and gradient-based optimisation algorithm is adopted, for $f=1,\dots,N$, to find the optimal variable matrix $\mathbf{X}(j\cdot\omega)$ by minimizing $\Phi_f\left(\mathbf{X}\right)$ [25-28] .The identification procedure at the f step utilizes the previously identified $\mathbf{X}(j\cdot\omega_{f-1})$ value as the starting point for the optimisation algorithm. The $\mathbf{X}(j\cdot\omega_f)$ estimates can be used to model the instrument frame dynamic behaviour at the ω_f frequency value, $f=1,\dots,N$.

Step 2: the $\mathbf{X}(j\cdot\omega))$ matrix coefficients can be modelled by means of a rational function formulation, since the instrument frame model can be associated to a classical second order, n_p poles mechanical system, i.e. by means of the ratio of a n_p-1 degree $p_{n_p-1}\left(j\cdot\omega\right)$ polynomial function to a n_p degree $p_{n_p}\left(j\cdot\omega\right)$ polynomial function, with real valued polynomial coefficients:

$$X_{rs}(j\cdot\omega) = \frac{a_{n_p-1}^{rs}\cdot P_{n_p-1}^{n_p-1}(j\cdot\omega) + \ldots + a_i^{rs}\cdot P_i^{n_p-1}(j\cdot\omega) + \ldots + a_0^{rs}\cdot P_0^{n_p-1}(j\cdot\omega)}{P_{n_p}^{n_p}(j\cdot\omega) + b_{n_p-1}\cdot P_{n_p-1}^{n_p}(j\cdot\omega) + \ldots + b_\ell\cdot P_\ell^{n_p}(j\cdot\omega) + \ldots + b_0\cdot P_0^{n_p}(j\cdot\omega)} \tag{19}$$

Where $P_i^{n_p-1}(j\cdot\omega)$, $i=0,\ldots,n_p-1$ and $P_\ell^{n_p}(j\cdot\omega)$, $\ell=0,\ldots,n_p$, and are polynomials from a known polynomial base, e.g. monomial, Legendre, Chebyshev, Forsythe among all [20,21], and $rs=(1,1)$, $(1,2)$ or $(2,2)$, where $X_{rs}(j\cdot\omega)$ is complex valued but a_i^{rs} and b_ℓ are all real valued coefficients.

Identification of n_p model order and a_i^{rs}, b_ℓ unknown coefficients can be done by means of well-known frequency based identification techniques [12], nevertheless complex a_i^{rs}, b_ℓ coefficients are expected to result from the application of such procedures. An extension of a procedure previously discussed by these same authors [4] is proposed and reported in appendix A, consisting in a linear real algebraic problem in real unknowns. The real a_i^{rs} and b_ℓ coefficients are identified by the procedure described in appendix A, with $n_q=3$, $G_1=X_{11}$, $G_2=X_{12}$, $G_3=G_{n_q}=X_{11}$, $m=n_p$, where the Legendre polynomial basis was chosen for $P_i^{m-1}(j\cdot\omega)$ and $P_\ell^m(j\cdot\omega)$ since the most accurate results were obtained with such choice.

4.Material model identification

A uniform slender beam specimen made of the material under study, coupled to the instrument frame is considered herein. The ratio of the transverse response to the force applied in the beam mobile end, in the frequency domain, is analytically known and can be inferred from Eq.(16). To identify the optimal $\mathbf{D}=\{D(j\cdot\omega_1)\quad\ldots\quad D(j\cdot\omega_N)\}$ values of the constitutive stress-strain relationship of the material in the measured $\boldsymbol{\omega}=\{\omega_1\quad\ldots\quad\omega_f\ldots\omega_N\}$ frequency range, a multi-step procedure is proposed.

Step 1: $D(j\cdot\omega)$ is first estimated by minimizing the scalar function Θ_f :

$$\Theta_f\left(D(j\cdot\omega_f)\right) = \left|H_f\left(D(j\cdot\omega_f)\right) - HM_f\right| \; ; \; f=1,\ldots,N \tag{20}$$

where HM_f is estimated from measurements and H_f from Eq. (16) depends on known $\mathbf{X}(j\cdot\omega)$ and exhibits a strong nonlinear dependency on $D(j\cdot\omega_f)$ (Eq.(11)). The optimisation approach used in §2,

step1 is here adopted to estimate $D(j \cdot \omega_f)$, $f = 1, \ldots, N$, with initial value conditions:

$$D(j \cdot \omega_1) = D(0) = 1, \ D(j \cdot \omega_f) = D(j \cdot \omega_{f-1}).$$

Step 2: from Eq.(3), the n_p poles rational fit model associated to $D(j \cdot \omega)$ results:

$$\frac{1}{D(j \cdot \omega)} = \frac{a_{n_K - 1} \cdot (j \cdot \omega)^{n_K - 1} + \ldots + a_1 \cdot (j \cdot \omega) + 1}{b_{n_p} \cdot (j \cdot \omega)^{n_K} + \ldots + b_1 \cdot (j \cdot \omega) + 1} = \frac{\dfrac{a_{n_K - 1}}{b_{n_K}} \cdot (j \cdot \omega)^{n_K - 1} + \ldots + \dfrac{a_1}{b_{n_K}} \cdot (j \cdot \omega) + \dfrac{1}{b_{n_K}}}{(j \cdot \omega)^{n_K} + \ldots + \dfrac{b_1}{b_{n_K}} \cdot (j \cdot \omega) + \dfrac{1}{b_{n_K}}} =$$

$$= \frac{c_{n_K - 1} \cdot (j \cdot \omega)^{n_K - 1} + \ldots + c_1 \cdot (j \cdot \omega) + c_0}{(j \cdot \omega)^{n_K} + d_{n_K - 1} \cdot (j \cdot \omega)^{n_K - 1} + \ldots + d_1 \cdot (j \cdot \omega) + d_0} \quad (21)$$

From Eq.(21) the $D(j \cdot \omega)$ reciprocal is expressed by a rational function expression consistent with Eq.(A.1). In order to identify the n_p, and a_i, b_ℓ coefficients optimal values, the procedure illustrated in Appendix A is adopted by choosing the following parameters: n_q=1, the Legendre polynomial basis and $c_0 \equiv d_0$. Unphysical and unstable poles are again eliminated by means of stability diagrams and the optimal $D(j \cdot \omega)$ rational model is obtained as a result.
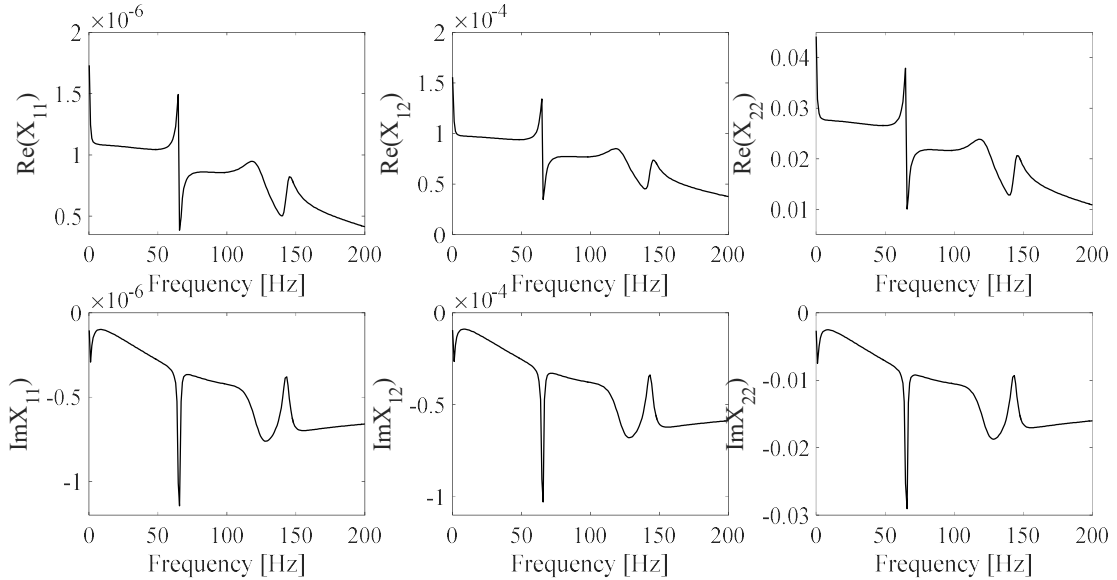

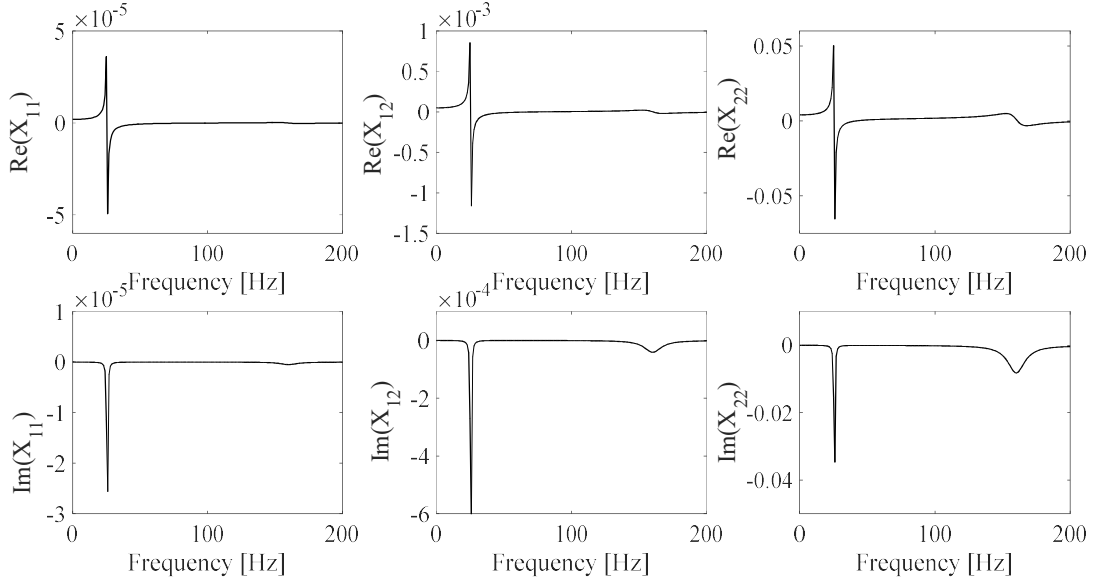**Fig.3**: IF1 $\mathbf{X}(\omega)$ assumed analytical model plot.

Fig.4: IF2 $\mathbf{X}(\omega)$ assumed analytical model plot.

5. Numerical and experimental test cases

5.1. Numerical test cases with simulated measurement noise

The optimization algorithm effectiveness is first evaluated by estimating the $\mathbf{X}(j \cdot \omega)$ model related to two numerically generated instrument frame analytical models, model IF1 (Fig.3) associated to 3 conjugated pole couples ($n_p = 6$) and model IF2 (Fig.4) associated to 2 conjugated pole couples ($n_p = 4$). In order to test the robustness of the proposed optimization algorithm, the contribution of random measurement noise was taken into account.

As previously indicated in section 3, in order to identify the $\mathbf{X}(j \cdot \omega)$ and $D(j \cdot \omega)$ models, measurements from reference beams are considered. When the optimization algorithm is applied to numerical test cases, measurement noise is simulated by adding random noise to the measurements obtained from the reference beams coupled to IF1 and IF2 frame analytical models. Virtual $HM_f^i = H_f^i \left(\mathbf{X}(j \cdot \omega_f) \right)$ measurements are then numerically simulated from the beam specimen test dataset related to beams 1-4, reported in Table 1, by means of Eq.(16) in the [0.1-200] Hz frequency range ($\omega_1 = 0.1$ Hz, $\omega_N = 200$ Hz, $N = 202$), without added noise and with added noise by assuming different signal to noise ratio values (S/N).
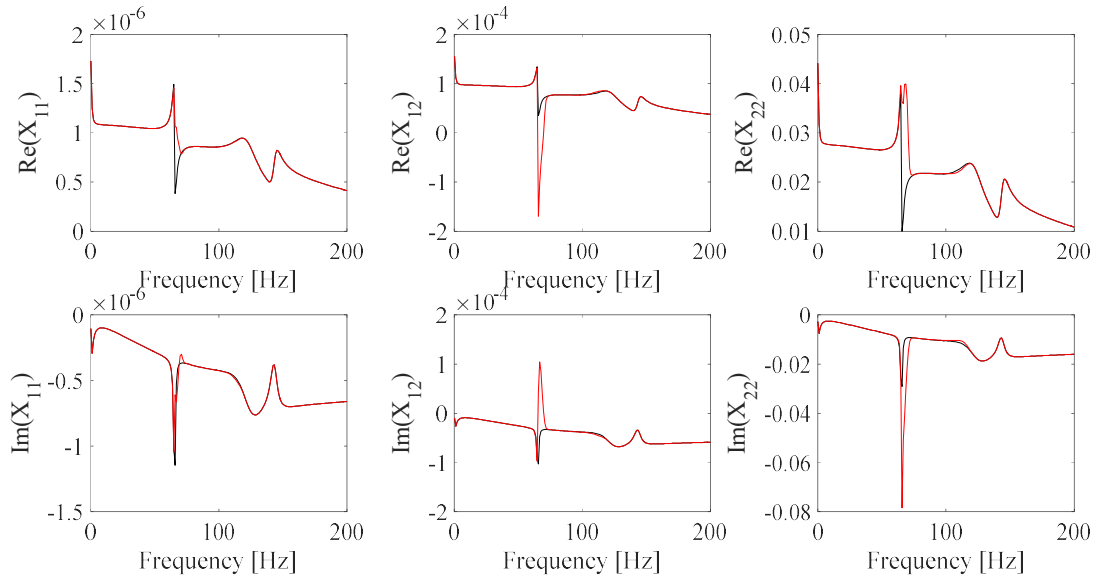
Fig.5: IF1 $\mathbf{X}(\omega)$ plot: (-black) reference, (- red) estimated values without added measurement noise.
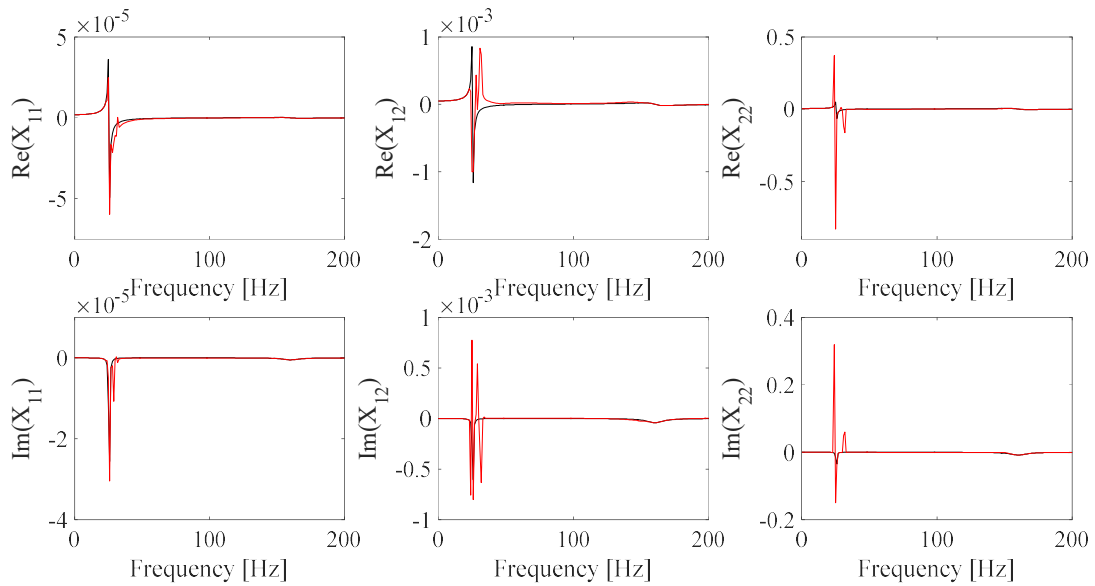

Fig.6: IF2 $\mathbf{X}(\omega)$ plot: (-black) reference, (- red) estimated values without added measurement noise.

Estimated $\mathbf{X}(j \cdot \omega)$ values, related to virtual measurements without added noise, are plotted in Figs.5-6, and the error associated to such estimated model is minimal.

Estimated $\mathbf{X}(j \cdot \omega)$ values, related to virtual measurements with added noise then follow. The $\left(HM_f^i \right)_{noise}$ simulated measurement results with noise are generated by means of the following equation:

$$\left(HM_f^i\right)_{noise} = HM_f^i + \sqrt{\frac{\left(\mathbf{HM}^i\right)^* \cdot \mathbf{HM}^i}{10^{\frac{S/N}{20}}}} \cdot e^{(2 \cdot \pi \cdot j \cdot Rand())}; \; f = 1, \ldots, N; \; i=1, \ldots, n_b \tag{22}$$

$$\mathbf{HM}^i = \left\{ HM_1 \quad \ldots \quad HM_f \quad \ldots \quad HM_N \right\}^T$$

where S/N is the selected noise signal to noise ratio expressed in dB and $Rand()$ is a function generating a random number between 0 and 1, and $.()^*$ is the conjugate transpose operator. Examples of the frequency response function measurements ($\left(HM_f^i\right)_{noise}$; $f = 1, \ldots, N$; i=1,$\ldots,n_b$) related to the IF2 generated instrument frame analytical model and obtained from beam 3 dataset (Table 1) with five different added noise levels ($S/N = 100, 90, 80, 70, 60$ dB) are presented in Fig.7. It must be taken into account that $S/N \geq 80$dB is typically expected in standard experimental test results, so that lower S/N values are here used to check the robustness of this novel identification approach.
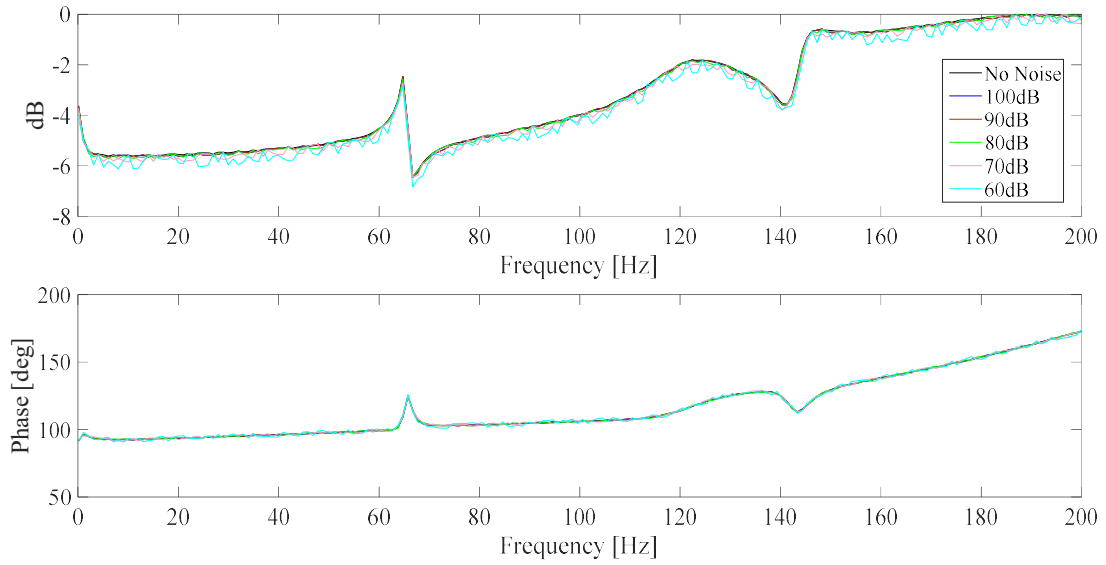

Fig.7: Numerically simulated FRF measurements related to beam 3 (IF1 frame model) without noise and with different added noise levels: $S/N = \left[60 \ldots 100\right]$dB.

$\mathbf{X}(j \cdot \omega_f)$ estimated results associated to the IF1 instrument frame analytical model from virtual measurements with different levels of added noise are reported in Figs.8-13 ($S/N = 60$ dB for Fig.8, $S/N = 70$ dB for Fig.9, $S/N = 80$ dB for Fig.10, $S/N = 90$ dB for Fig.11, $S/N = 100$ dB for Fig.12). The results show that the optimization procedure is able to effectively identify the unknown frame model even if high levels of measurement noise are taken into account. $\mathbf{X}(j \cdot \omega_f)$ estimated results

associated to the IF2 instrument frame analytical model from virtual measurements with $S/N = 80$ dB added noise are reported in Fig.13, being again fully consistent with the theoretical model.

Rational fits are then identified by adopting the procedure illustrated in section 3, and results are plotted in Figs.8-12 (IF1) and Fig.13 (IF2), showing a good consistency with theoretical expected values.
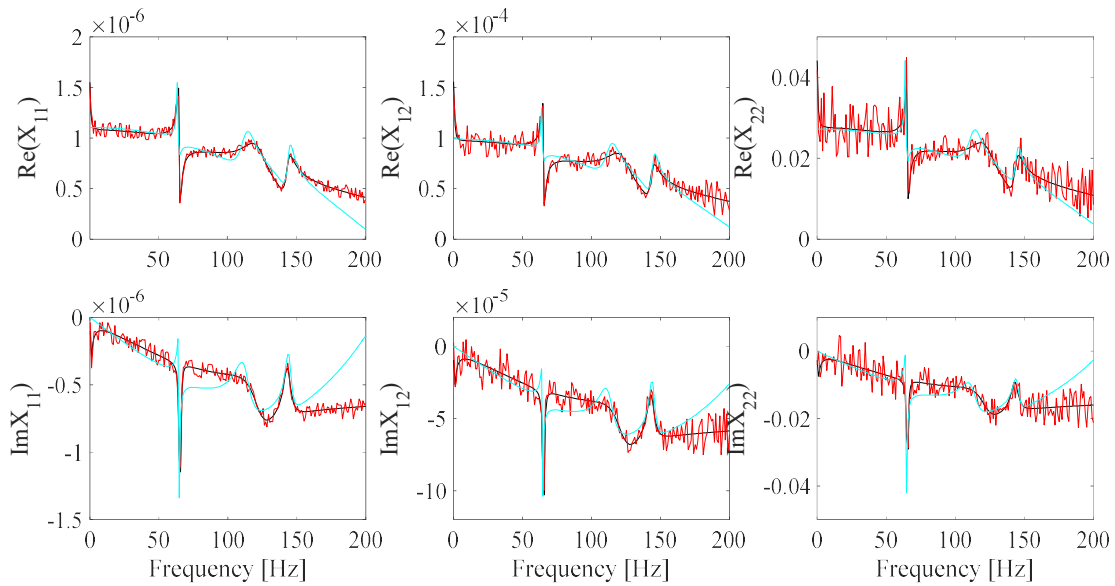

Fig.8: IF1 $\mathbf{X}(\omega)$ estimates: (- black) reference, (- red) estimated values and (- cyan) $n_p = 6$ rational fit with added measurement noise ($S/N = 60\text{dB}$).
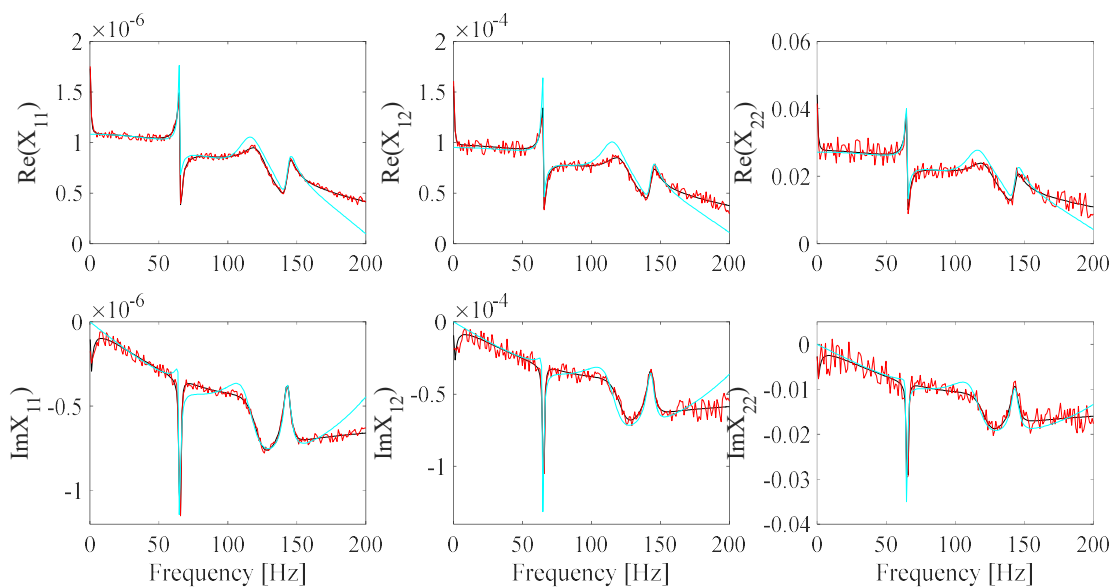
Fig.9: IF1 $\mathbf{X}(\omega)$ estimates: (- black) reference, (- red) estimated values and (- cyan) $n_p = 6$ rational fit with added measurement noise ($S/N = 70dB$).
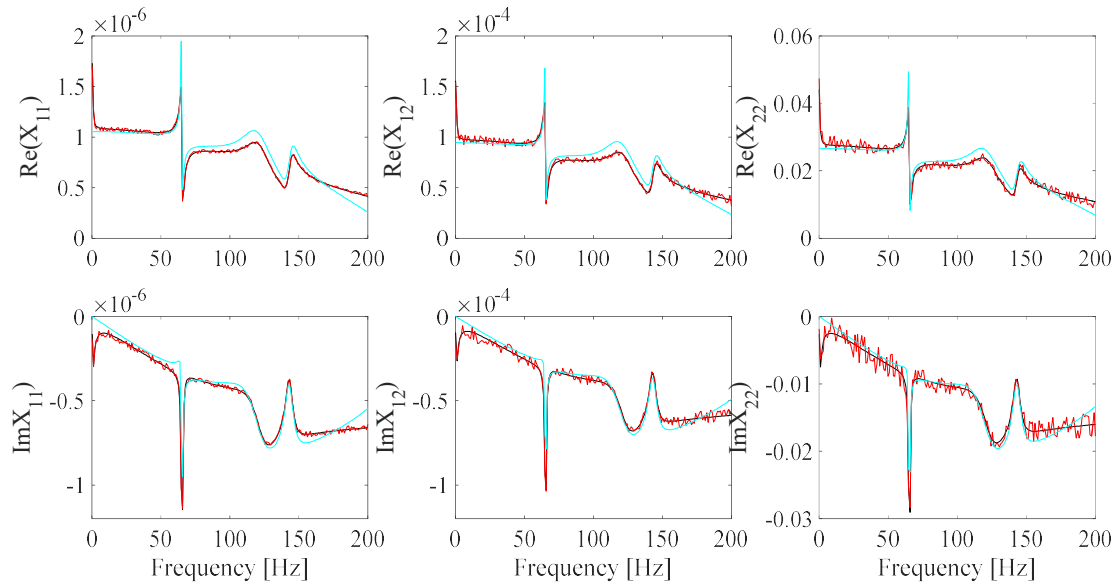

Fig.10: IF1 $\mathbf{X}(\omega)$ estimates: (- black) reference, (- red) estimated values and (- cyan) $n_p = 6$ rational fit with added measurement noise ($S/N = 80dB$).
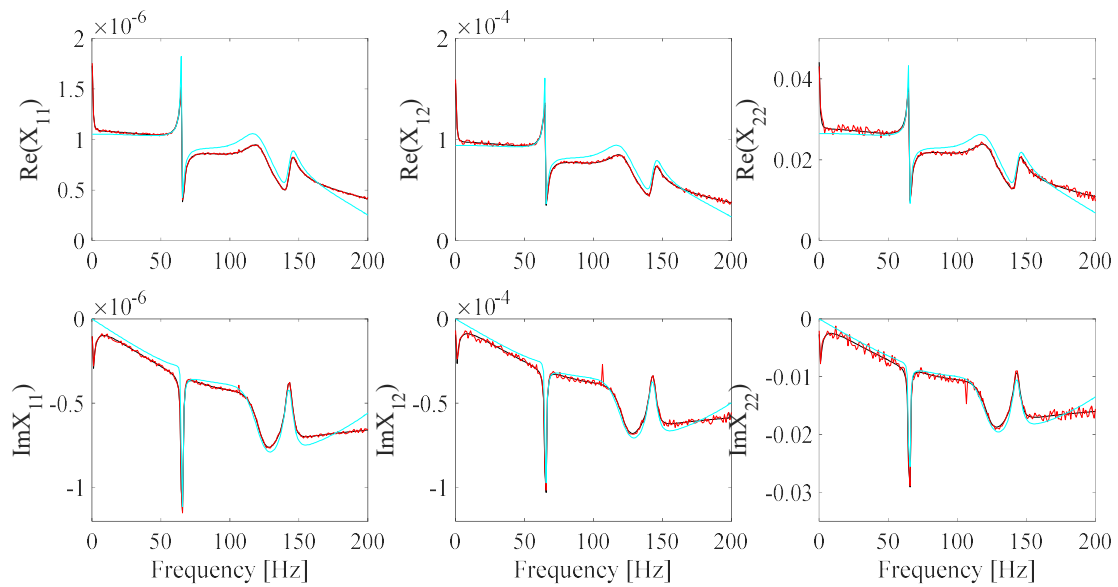

Fig.11: IF1 $\mathbf{X}(\omega)$ estimates: (- black) reference, (- red) estimated values and (- cyan) $n_p = 6$ rational fit with added measurement noise ($S/N = 90dB$).
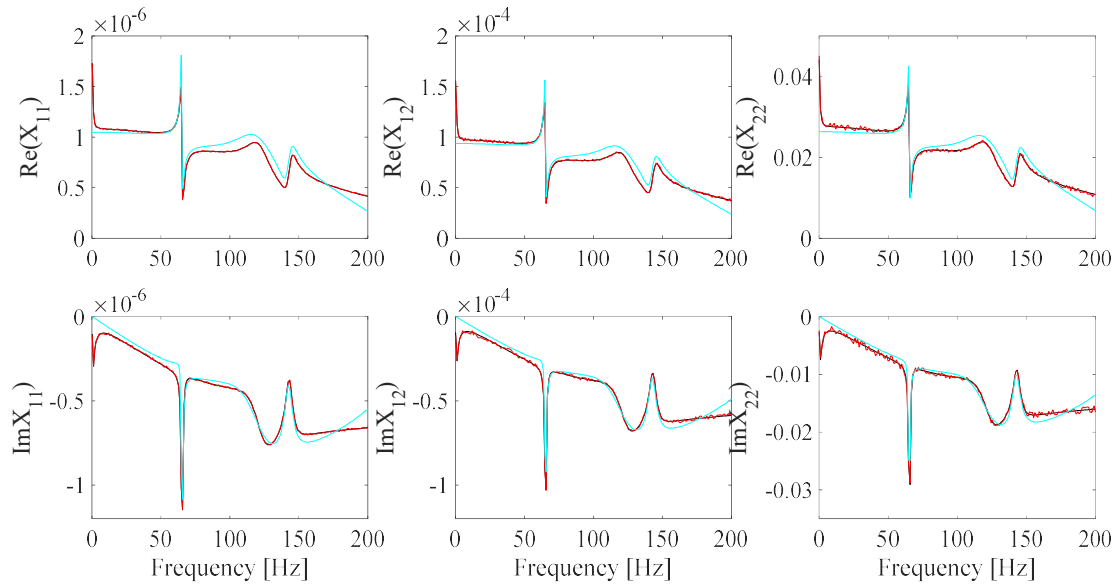
Fig.12: IF1 $\mathbf{X}(\omega)$ estimates: (- black) reference, (- red) estimated values and (- cyan) $n_p = 6$ rational fit with added measurement noise ($\mathrm{S/N} = 100\mathrm{dB}$).
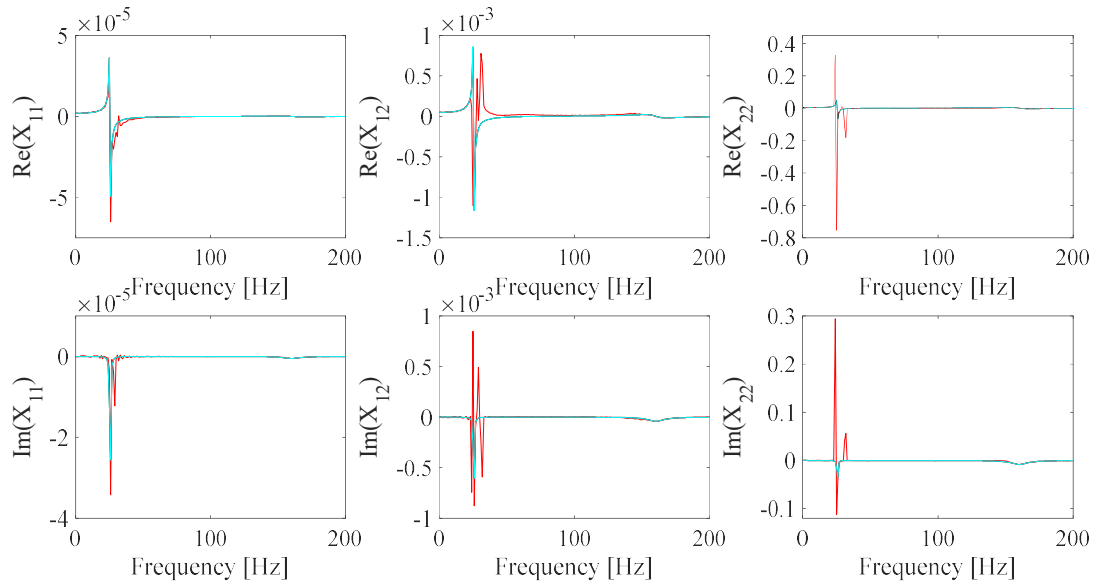

Fig.13: IF2 $\mathbf{X}(\omega)$ estimates: (- black) reference, (- red) estimated values and (- cyan) $n_p = 4$ rational fit with added measurement noise ($\mathrm{S/N} = 80\mathrm{dB}$).

The material identification procedure is then tested from simulated HM_f measurements obtained from the beam specimen dataset 5 reported in Table 1, with $\mathrm{S/N} = 80$ dB added noise, in the [0.1-200] Hz frequency range ($\omega_1 = 0.1$ Hz, $\omega_N = 200$ Hz, $N = 202$), by using the identified rational fit (Figs.10,13

S/N = 80 dB) related to both IF1 and IF2 models, previously identified from measurements with

S/N = 80 dB added noise. The effectiveness of the $D(j \cdot \omega)$ optimization and rational fit identification

procedures is tested and results are shown in Figs.14-15. The $D(j \cdot \omega)$ rational model obtained with

respect to both IF1 and IF2 instrument frame assumed configurations is the same, showing $n_k = 0$, and

being consistent with the $D(j \cdot \omega)$ theoretical Hooke model assumed for beam 5 (Table 1). The

identification results related to the rigid frame assumption ($\mathbf{X}(j \cdot \omega) = \mathbf{0}$) are reported as well, showing

that the dynamic contribution of the frame may seriously affect the $D(j \cdot \omega)$ model estimate in practical

test applications.

Table 1: Beam specimens data used for $\mathbf{X}(\omega)$, $D(\omega)$ identification (numerical test cases)

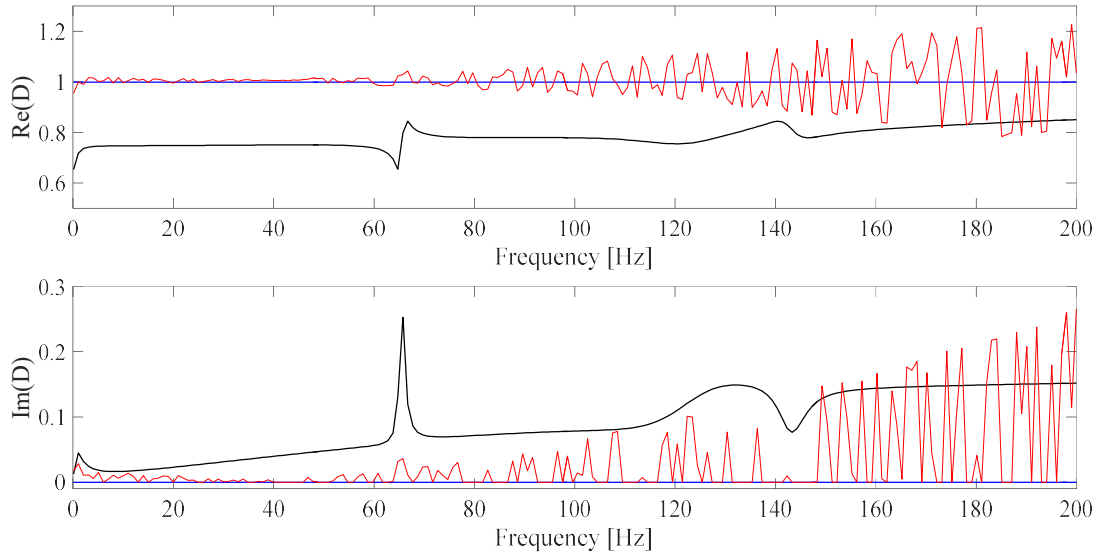| Beam	Length (m)	Thickness (m)	Width (m)	Density (kg/m³)	E_0 (Pa)	$D(\omega)$ model
1	$1.75 \cdot 10^{-2}$	$0.75 \cdot 10^{-3}$	$12.7 \cdot 10^{-3}$	7850	$2.1 \cdot 10^{11}$	Hooke ($D(j \cdot \omega)$=1)
2	$1.75 \cdot 10^{-2}$	$3.0 \cdot 10^{-3}$	$3.0 \cdot 10^{-3}$	7850	$2.1 \cdot 10^{11}$	Hooke ($D(j \cdot \omega)$=1)
3	$1.75 \cdot 10^{-2}$	$3.0 \cdot 10^{-3}$	$5.0 \cdot 10^{-3}$	7850	$2.1 \cdot 10^{11}$	Hooke ($D(j \cdot \omega)$=1)
4	$1.75 \cdot 10^{-2}$	$5.0 \cdot 10^{-3}$	$3.0 \cdot 10^{-3}$	7850	$2.1 \cdot 10^{11}$	Hooke ($D(j \cdot \omega)$=1)
5	$1.75 \cdot 10^{-2}$	$0.5 \cdot 10^{-3}$	$3.0 \cdot 10^{-3}$	7850	$2.1 \cdot 10^{11}$	Hooke ($D(j \cdot \omega)$=1)

Fig.14: beam 5 material $D(j \cdot \omega))$ estimate from IF1 frame measurements with noise ($S/N = 80dB$):
(- black) Step 1 with $\mathbf{X}(\omega) = \mathbf{0}$ assumption; (- red) Step 1 with $\mathbf{X}(\omega)$ $n_p = 6$ rational fit model; (- blue) Step 2 ($n_k = 0$) with $\mathbf{X}(\omega)$ $n_p = 6$ rational fit model.

Fig.15: beam 5 material $D(j \cdot \omega))$ estimate from IF2 frame measurements with noise ($S/N = 80dB$):
(- black) Step 1 with $\mathbf{X}(\omega) = \mathbf{0}$ assumption; (- red) Step 1 with $\mathbf{X}(\omega)$ $n_p = 4$ rational fit model;
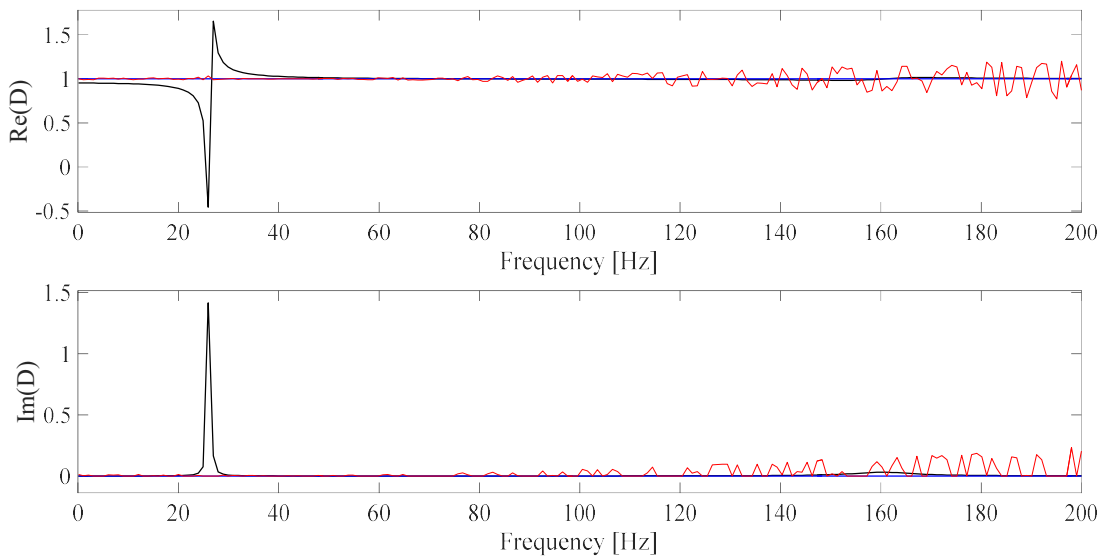(- blue) Step 2 ($n_k = 0$) with $\mathbf{X}(\omega)$ $n_p = 4$ rational fit model.
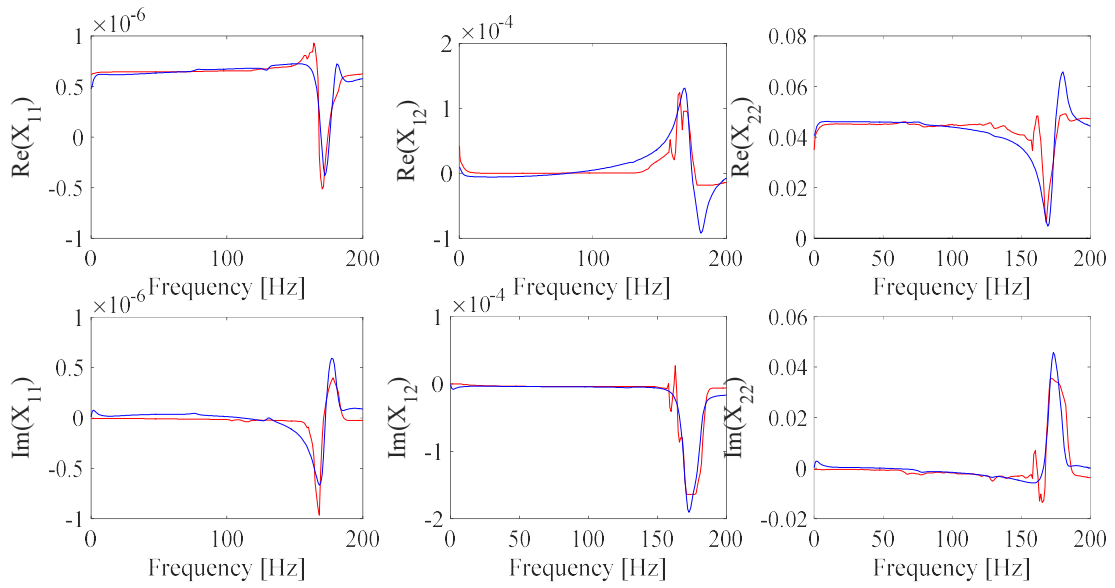
Fig.16: $X_{11}(j\cdot\omega), X_{12}(j\cdot\omega)$, $X_{22}(j\cdot\omega)$ estimated values: (- red) Step 1; (- blue) Step 2 $n_p = 12$ rational fit.

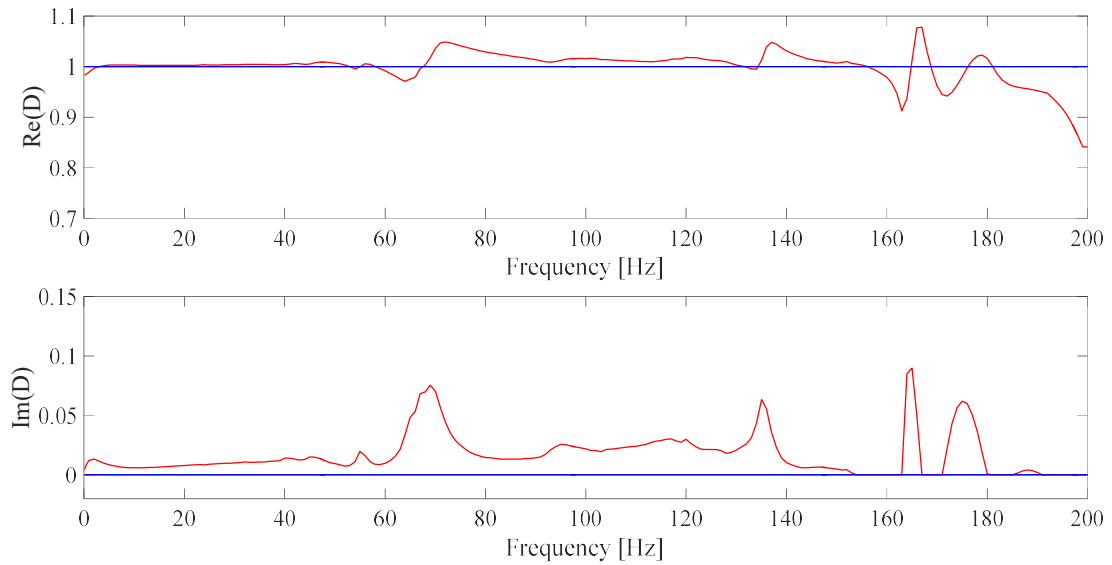**Fig.17**: beam 5 $D(j\cdot\omega)$ estimates: (- red) Step 1; (- blue) Step 2 $n_k = 0$ rational fit.
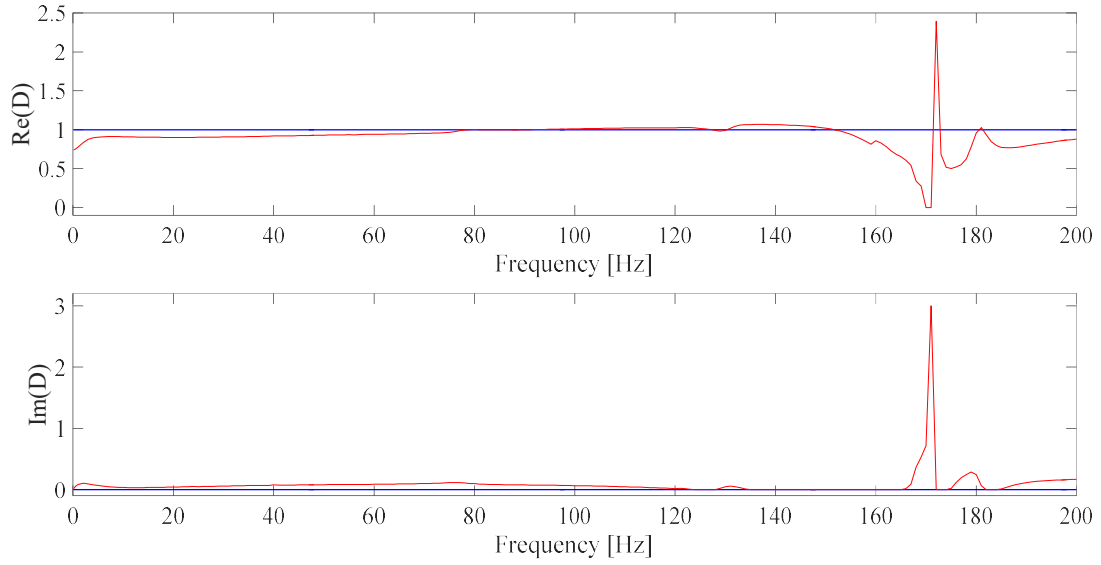
Fig.18: beam 6 $D(j \cdot \omega)$ estimates: (- red) Step 1; (- blue) Step 2 $n_k = 0$ rational fit.
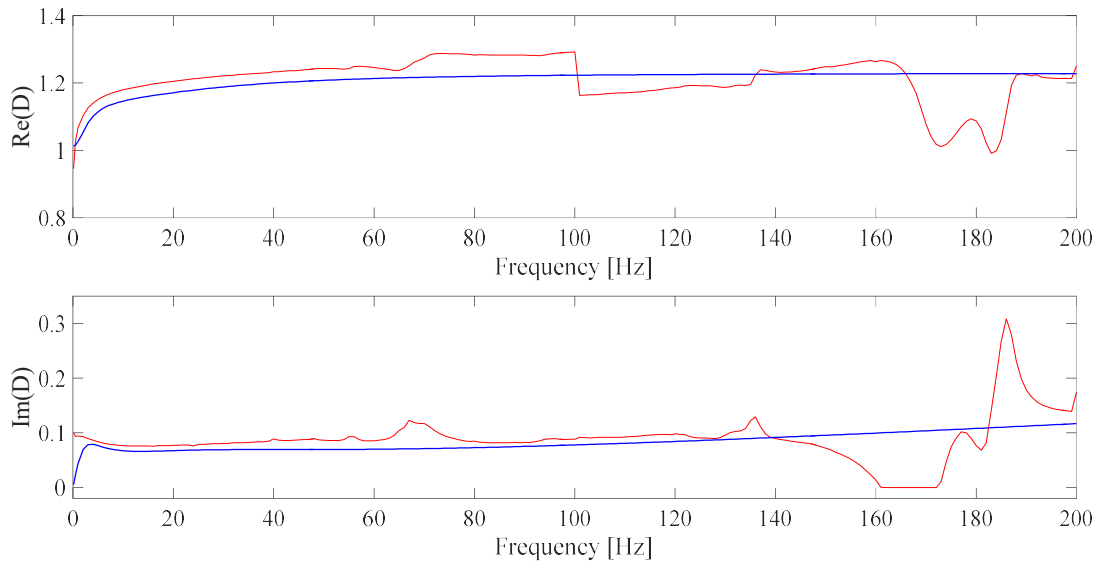
Fig.19: beam 7 $D(j \cdot \omega)$ estimates: (- red) Step 1; (- blue) Step 2 $n_k = 3$ rational fit.

5.2. Experimental test cases

The $\mathbf{X}(j \cdot \omega)$ and $D(j \cdot \omega)$ identification procedures are then applied to true experimental measurements made with an industrially available DMA measuring systems (TA instruments DMA Q800). The experimental set-up is the one outlined in Fig.2. All measurements were made in the low strain amplitude range ($\varepsilon_{max} < 1.5 \cdot 10^{-4}$), 202 frequency steps ($\omega_1 = 0.1$ Hz, $\omega_N = 200$ Hz, $N = 202$), constant temperature ($T = 35\,°C$) experimental conditions. A set of four reference beam specimens (

$n_b = 4$) made of the same harmonic steel material but different geometry, so that different flexural stiffness is taken into account is used to estimate the instrument frame $\mathbf{X}(j \cdot \omega_f)$. Beam specimen data values are reported in Table 2 (beam 1-4). The identified $\mathbf{X}(j \cdot \omega_f)$ element matrix estimates resulting from the two steps identification procedure are plotted with respect to frequency in Fig.16. Optimal model order $n_p = 12$ results from the $\mathbf{X}(j \cdot \omega)$ rational fit identification procedure (Step 2). The unknown material model of beams 5,6,7, whose known parameters (E_0, ρ) are reported in Table.2, is then identified from within measurements made specimens whose parameters are again reported in Table 2. The $D(j \cdot \omega)$ proposed identification technique is applied by assuming the $n_p = 12$ previously identified rational fit $\mathbf{X}(j \cdot \omega)$ frame model.

Fig.20: beam 5 $D(j \cdot \omega)$ estimates: (- blue) Step 2 $n_k = 0$ rational fit.; (- green) Step 2 $\mathbf{X}(\omega) = \mathbf{0}$ $n_k = 5$ rational fit.
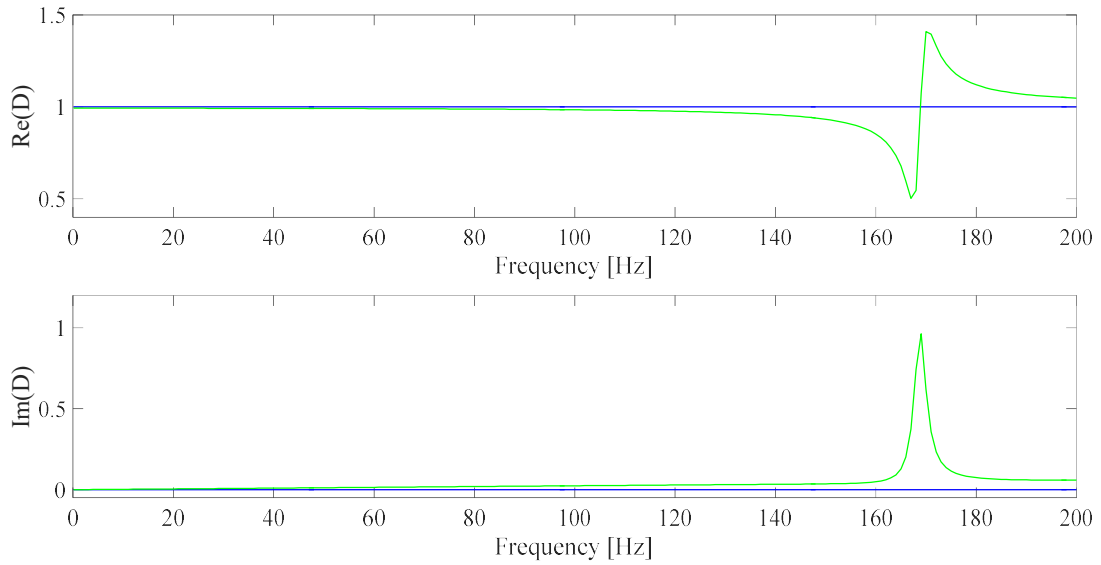
Fig.21: beam 6 $D(j \cdot \omega)$ estimates: (- blue) Step 2 $n_k = 0$ rational fit.; (- green) Step 2 $\mathbf{X}(\omega) = \mathbf{0}$ $n_k = 3$ rational fit.
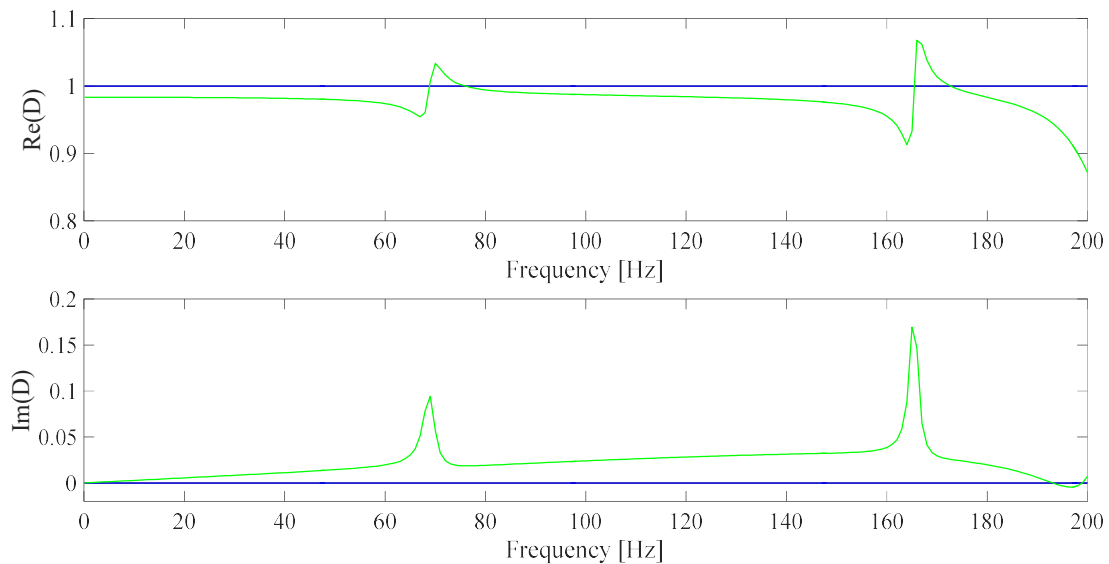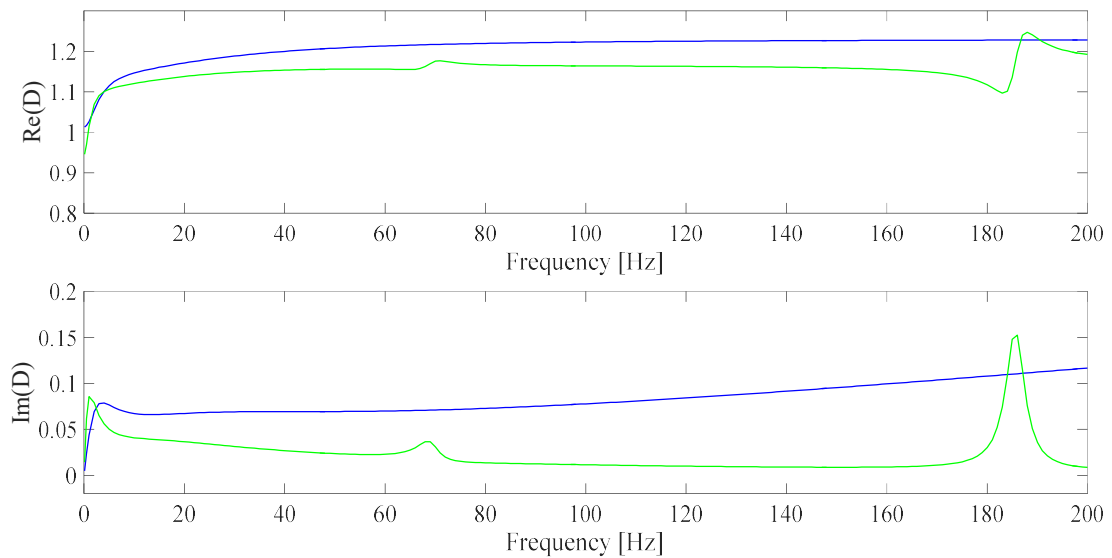

Fig.22: beam 7 $D(j \cdot \omega)$ estimates: (- blue) Step 2 $n_k = 0$ rational fit.; (- green) Step 2 $\mathbf{X}(\omega) = \mathbf{0}$ $n_k = 6$ rational fit.

The estimated $D(j \cdot \omega_f)$ values related to beam 5-7 specimens are reported in Figs.17-19, where results associated to the Step 1 and Step 2 identification procedures are outlined. It appears that the results concerning the beam 5-6 harmonic steel material are consistent with the expected Hooke model (no

poles, $n_k = 0$), while a physically sound optimal $n_k = 3$ material model, 3 real poles, is obtained for the epoxy-resin (Epostick®) specimen (beam 7). Figs.20-22 compare the material $D(j \cdot \omega_f)$ identified results related to beam 5-7 specimens, obtained by adopting standard assumptions, i.e. assuming a rigid instrument frame $\mathbf{X}(j \cdot \omega_f) = \mathbf{0}$, with the corresponding results obtained by using the procedure underlined in this work. It appears that the frame contribution has a noticeable effect on all of the identified estimates related to different materials, so that the added experimental and processing burden associated to the approach described in this work appears to be justified.

Table 2: Beam specimens data used for $\mathbf{X}(j \cdot \omega)$, $D(j \cdot \omega)$ identification (experimental test cases)

Beam	Material	Length (m)	Thickness (m)	Width (m)	Density (kg/m³)	E_0 (Pa)
1	C67 harmonic steel	$(1.75 \pm 0.001) \cdot 10^{-2}$	$(0.75 \pm 0.01) \cdot 10^{-3}$	$(12.7 \pm 0.01) \cdot 10^{-3}$	7850 ± 5	$(2.1 \pm 0.5) \cdot 10^{11}$
2	C67 harmonic steel	$(1.75 \pm 0.001) \cdot 10^{-2}$	$(3.0 \pm 0.01) \cdot 10^{-3}$	$(3.0 \pm 0.01) \cdot 10^{-3}$	7850 ± 5	$(2.1 \pm 0.5) \cdot 10^{11}$
3	C67 harmonic steel	$(1.75 \pm 0.001) \cdot 10^{-2}$	$(3.0 \pm 0.01) \cdot 10^{-3}$	$(5.0 \pm 0.01) \cdot 10^{-3}$	7850 ± 5	$(2.1 \pm 0.5) \cdot 10^{11}$
4	C67 harmonic steel	$(1.75 \pm 0.001) \cdot 10^{-2}$	$(5.0 \pm 0.01) \cdot 10^{-3}$	$(3.0 \pm 0.01) \cdot 10^{-3}$	7850 ± 5	$(2.1 \pm 0.5) \cdot 10^{11}$
5	C67 harmonic steel	$(1.75 \pm 0.001) \cdot 10^{-2}$	$(0.5 \pm 0.01) \cdot 10^{-3}$	$(13.8 \pm 0.01) \cdot 10^{-3}$	7850 ± 5	$(2.1 \pm 0.5) \cdot 10^{11}$
6	C67 harmonic steel	$(1.75 \pm 0.001) \cdot 10^{-2}$	$(4.0 \pm 0.01) \cdot 10^{-3}$	$(3.0 \pm 0.01) \cdot 10^{-3}$	7850 ± 5	$(2.1 \pm 0.5) \cdot 10^{11}$
7	Commercial epoxy-resin (Epostick®)	$(1.75 \pm 0.001) \cdot 10^{-2}$	$(1.5 \pm 0.01) \cdot 10^{-3}$	$(5.8 \pm 0.01) \cdot 10^{-3}$	2500 ± 5	$(4.0 \pm 0.1) \cdot 10^{9}$

Conclusions

A robust identification procedure able to estimate the material model rational fit i the frequency domain, by eliminating unwanted components due to model noise associated to the instrument frame contribution and also to measurement noise is presented in this work. The proposed technique relies on standard forced sinusoidal excitation measurements made on beam specimens realized with the material under study, as available in most commercially known test systems. A novel identification technique is here proposed to filter the contributions of model and experimental noise. By assuming that the material follows a n_k order generalized Kelvin model, a rational polynomial analytical model is assumed as well, and the optimal model order and parameters are identified with the proposed approach. The technique does take into account of the contribution of the instrument frame onto the measurement results to increase the accuracy of the material $D(j \cdot \omega)$ identified results. Since polynomial rational models with real coefficients are expected to model both the $\mathbf{X}(j \cdot \omega)$ instrument frame and the $D(j \cdot \omega)$ material, an extended procedure consisting in a linear real algebraic problem in real unknowns is defined to obtain the model unknowns, and reported in the Appendix.

Numerical test case results are reported to show the robustness of the identification procedures used to estimate the instrument frame and the material $D(j \cdot \omega)$ models. Experimental test cases are then presented, and the instrument frame model of a real industrially available test system is modelled by means of a high order rational model and the rational material model of harmonic steel beams of different geometry is accurately identified and a Hooke material model results. The model identification of a dual component epoxy resin, whose model is unknown, is then obtained, and the results are shown.

These results are then compared with the identification results obtained by adopting standard assumptions, i.e. assuming a rigid instrument frame $\mathbf{X}(j \cdot \omega_f) = \mathbf{0}$, showing that the frame contribution cannot be neglected in pratical applications, and justifying the approach described in this work.

It must be outlined that the identification results strongly depend on the accuracy of the identified instrument frame model associated to the measurement frequency range. To increase the frame model accuracy, the force and displacement measurement precision, the data acquisition resolution, the frequency range, the number of experimental dofs should be increased as well. Nevertheless, since the main task of this work consists in only employing the minimal set of data measurements available in a

typical commercially available DMA test system, it is beyond the scope of this paper to investigate a different measuring test strategy.

APPENDIX A: Rational MDOF FRF frequency domain identification technique

The $G_q(j \cdot \omega)$ FRF functions related to a 2nd order, m poles mechanical model, can be expressed as follows:

$$G_q(j \cdot \omega) = \sum_{i=1}^{m} \frac{R_i^q}{j\omega - p_i} = \frac{\sum_{i=0}^{m-1} a_i^q \cdot P_i^{m-1}(j \cdot \omega)}{P_m^m(j \cdot \omega) + \sum_{\ell=0}^{m-1} b_\ell \cdot P_\ell^m(j \cdot \omega)};$$ (A.1)

where $G_q(j \cdot \omega_f)$ are complex measurement FRF estimates, $q = 1,\ldots,n_q$, $f = 1,\ldots,N$, and $R_i^q, p_i \in \mathbb{C}$, $a_i^q, b_\ell \in \mathbb{R}$, q index being referred to the r output, s input dofs couple taken into account. $P_i^{m-1}(j \cdot \omega)$ and $P_\ell^m(j \cdot \omega)$ are polynomials from a known polynomial base, e.g. monomial, Legendre, Chebyshev among all [20,21]. Frequency domain model identification consists in finding unknown $2 \times m$ a_i^q, b_ℓ real values or R_i^q, p_i complex values generally resulting in complex conjugate pairs. It must be outlined that b_ℓ, p_i are common to every q or r, s experimental dof input-output couple, i.e. do not vary with respect to q, while R_i^q, a_i^q are strictly dependent on q.

Since $G_q \in \mathbb{C}$:

$$G_q(j \cdot \omega) = \mathrm{Re}\big(G_q(j \cdot \omega)\big) + j \cdot \mathrm{Im}\big(G_q(j \cdot \omega)\big).$$ (A.2)

A n grade, $n+1$ order, polynomial can be expressed as:

$$\tau_n(j \cdot \omega) = \sum_{i=0}^{n} c_k \cdot P_k^n(j \cdot \omega) = c_0 \cdot P_0^n(j \cdot \omega) + \ldots + c_n \cdot P_n^n(j \cdot \omega)$$ (A.3)

By normalizing the ω range, putting $u = \dfrac{\omega}{\omega_N}$ and $n2$=floor($n/2$):

$$P_k^n(j \cdot \omega) = j^k \cdot \omega_N^k \cdot P_k^n(u)$$

$$\begin{cases} P_k^n(j \cdot \omega) = (-1)^{\frac{k}{2}} \cdot \omega_N^k \cdot P_k^n(-u) & , \quad \text{when } k \text{ is even} \\ P_k^n(j \cdot \omega) = j \cdot (-1)^{\frac{k-1}{2}} \cdot \omega_N^k \cdot P_k^n(u) & , \quad \text{when } k \text{ is odd} \end{cases}$$ (A.4)

if n is even:

$$\tau_n = \sum_{k=0}^{n2} c_{2k} \cdot (-1)^k \cdot \omega_N^{2k} \cdot P_{2k}^n(u) + j \cdot \sum_{k=0}^{n2-1} c_{2k+1} \cdot (-1)^k \cdot \omega_N^{2k+1} \cdot P_{2k+1}^n(u) = \sum_{k=0}^{n2} \varphi_k \cdot \Pi_k^n(u) + j \cdot \sum_{k=0}^{n2-1} \eta_k \cdot \Lambda_k^n(u),$$

$$\varphi_k = c_{2k} \cdot (-1)^k \cdot \omega_N^{2k} \; ; \quad \Pi_k^n(u) = P_{2k}^n(u) \; ; \tag{A.5}$$

$$\eta_k = c_{2k+1} \cdot (-1)^k \cdot \omega_N^{2k+1} \; ; \quad \Lambda_k^n(u) = P_{2k+1}^n(u);$$

If n is odd:

$$\tau_n = \sum_{k=0}^{n2} c_{2k} \cdot (-1)^k \cdot \omega_N^{2k} \cdot P_{2k}^n(u) + j \cdot \sum_{k=0}^{n2} c_{2k+1} \cdot (-1)^k \cdot \omega_N^{2k+1} \cdot P_{2k+1}^n(u) = \sum_{k=0}^{n2} \varphi_k \cdot \Pi_k^n(u) + j \cdot \sum_{k=0}^{n2} \eta_k \cdot \Lambda_k^n(u) \tag{A.6}$$

In a more compact vector form:

$$\tau_n = \mathbf{\Pi}^n \cdot \mathbf{\varphi} + j \cdot \mathbf{\Lambda}^n \cdot \mathbf{\eta}$$

$$\mathbf{\Pi}^n = \left\{ \Pi_0^n(u) \quad \ldots \quad \Pi_{n_\Pi -1}^n(u) \right\} \; , \quad \mathbf{\Lambda}^n = \left\{ \Lambda_0^n(u) \quad \ldots \quad \Lambda_{n_\Lambda -1}^n(u) \right\}$$

$$\mathbf{\varphi} = \left\{ \varphi_0 \quad \ldots \quad \varphi_{n_\Pi -1} \right\}^T \; , \quad \mathbf{\eta} = \left\{ \eta_0 \quad \ldots \quad \beta_{n_\Lambda -1} \right\}^T \tag{A.7}$$

$$n_\Pi = \left| \frac{n+1}{2} \right|_{+\infty} = ceil\left(\frac{n+1}{2} \right) \; , \quad n_\Lambda = \left| \frac{n+1}{2} \right|_{-\infty} = floor\left(\frac{n+1}{2} \right)$$

$$n_\Pi + n_\Lambda = n+1$$

From Eqs.(A.1,A.4-A.7):

$$G_q(j \cdot \omega) = \frac{\mathbf{A}^{m-1} \cdot \mathbf{\alpha}^q + j \cdot \mathbf{B}^{m-1} \cdot \mathbf{\beta}^q}{\left[1 - \mathrm{mod}(m,2) \right] \cdot P_m^m(j \cdot \omega) + \mathbf{C}^{m-1} \cdot \mathbf{\gamma} + j \cdot \left[\mathrm{mod}(m,2) \cdot P_m^m(j \cdot \omega) + \mathbf{O}^{m-1} \cdot \mathbf{\mu} \right]} \tag{A.8}$$

$$\mathbf{A}^{m-1}, \mathbf{C}^{m-1} \in \mathbb{R}^{1 \times \left| \frac{m}{2} \right|_{+\infty}} \; ; \quad \mathbf{\alpha}^q, \mathbf{\gamma} \in \mathbb{R}^{1 \times \left| \frac{m}{2} \right|_{+\infty}} \; ; \quad \mathbf{B}^{m-1}, \mathbf{O}^{m-1} \in \mathbb{R}^{1 \times \left| \frac{m}{2} \right|_{-\infty}} \; ; \quad \mathbf{\beta}^q, \mathbf{\mu} \in \mathbb{R}^{1 \times \left| \frac{m}{2} \right|_{-\infty}}$$

where $\mathbf{A}^{m-1}, \mathbf{B}^{m-1}, \mathbf{\alpha}^q, \mathbf{\beta}^q$ and $\mathbf{C}^{m-1}, \mathbf{O}^{m-1}, \mathbf{\gamma}, \mathbf{\mu}$ are defined as in Eq.(A.7). From Eq.(A.8):

$$\begin{aligned}
\mathbf{A}^{m-1} \cdot \mathbf{\alpha}^q + j \cdot \mathbf{B}^{m-1} \cdot \mathbf{\beta}^q ={}& \mathrm{Re}\left(G_q(j \cdot \omega) \right) \cdot \left[1 - \mathrm{mod}(m,2) \right] \cdot P_m^m(j \cdot \omega) + \mathrm{Re}\left(G_q(j \cdot \omega) \right) \cdot \mathbf{C}^{m-1} \cdot \mathbf{\gamma} + \\
&- \mathrm{Im}\left(G_q(j \cdot \omega) \right) \cdot \mathrm{mod}(m,2) \cdot P_m^m(j \cdot \omega) - \mathrm{Im}\left(G_q(j \cdot \omega) \right) \cdot \mathbf{O}^{m-1} \cdot \mathbf{\mu} + \\
&+ j \cdot \left\{ \mathrm{Im}\left(G_q(j \cdot \omega) \right) \cdot \left[1 - \mathrm{mod}(m,2) \right] \cdot P_m^m(j \cdot \omega) + \mathrm{Im}\left(G_q(j \cdot \omega) \right) \cdot \mathbf{C}^{m-1} \cdot \mathbf{\gamma} + \right. \\
&\left. + \mathrm{Re}\left(G_q(j \cdot \omega) \right) \cdot \mathrm{mod}(m,2) \cdot P_m^m(j \cdot \omega) - \mathrm{Re}\left(G_q(j \cdot \omega) \right) \cdot \mathbf{O}^{m-1} \cdot \mathbf{\mu} \right\}
\end{aligned} \tag{A.9}$$

From Eq.(A.9), and taking into account that $G_q(j \cdot \omega)$ are estimated with respect to discrete

$\omega_f, f = 1, \ldots, N$ values:

$$\begin{cases}
\mathbf{AN}^{m-1} \cdot \boldsymbol{\alpha}^q - \left[\operatorname{Re}(\mathbf{GN}_q) \cdot \mathbf{C}^{m-1} \right] \cdot \boldsymbol{\gamma} + \left[\operatorname{Im}(\mathbf{GN}_q) \cdot \mathbf{O}^{m-1} \right] \cdot \boldsymbol{\mu} = \\
\qquad = \left\{ P_m^m \cdot \left[\operatorname{Re}(\mathbf{GN}_q) - \operatorname{mod}(m,2) \cdot \left(\operatorname{Re}(\mathbf{GN}_q) + \operatorname{Im}(\mathbf{GN}_q) \right) \right] \right\} \\
\mathbf{BN}^{m-1} \cdot \boldsymbol{\beta}^q - \left[\operatorname{Im}(\mathbf{GN}_q) \cdot \mathbf{C}^{m-1} \right] \cdot \boldsymbol{\gamma} - \left[\operatorname{Re}(\mathbf{GN}_q) \cdot \mathbf{O}^{m-1} \right] \cdot \boldsymbol{\mu} = \\
\qquad = \left\{ P_m^m \cdot \left[\operatorname{Im}(\mathbf{GN}_q) + \operatorname{mod}(m,2) \cdot \left(\operatorname{Re}(\mathbf{GN}_q) - \operatorname{Im}(\mathbf{GN}_q) \right) \right] \right\}
\end{cases}$$

$$\mathbf{GN}_q = \left\{ G_q(j \cdot \omega_1) \quad \dots \quad G_q(j \cdot \omega_N) \right\}^T \tag{A.10}$$

$$\mathbf{AN}^{m-1} \in \mathbb{R}^{N \times nA} \quad, \quad \mathbf{BN}^{m-1} \in \mathbb{R}^{N \times nB}$$

Eq.(A10) refers to a set of $2 \times n_q \times N$ linear real algebraic problem in $(n_q + 1) \times m$ real unknowns ($\boldsymbol{\alpha}^q, \boldsymbol{\beta}^q, \boldsymbol{\gamma}, \boldsymbol{\mu}$, $q = 1, \dots, n_q$). Since $N \gg m$, an oversized linear system results, and can be solved by means of a Least Square minimization technique.

From Eq. (A.10), $\mathbf{e}_1$ and $\mathbf{e}_2$ error vectors, associate to the real and imaginary part of Eq.(A.9) can be defined:

$$\begin{cases}
\mathbf{AN} \cdot \boldsymbol{\alpha} - \mathbf{H} \cdot \boldsymbol{\gamma} - \mathbf{K} \cdot \boldsymbol{\mu} - \mathbf{b}_1 = \mathbf{e}_1 \\
\mathbf{BN} \cdot \boldsymbol{\beta} - \mathbf{T} \cdot \boldsymbol{\gamma} - \mathbf{S} \cdot \boldsymbol{\mu} - \mathbf{b}_2 = \mathbf{e}_2
\end{cases} \tag{A.11}$$

Where:

$$\mathbf{AN} = \begin{bmatrix} \mathbf{AN}^{m-1} & \mathbf{0} & \dots & 0 & 0 \\ 0 & \mathbf{AN}^{m-1} & \dots & 0 & 0 \\ \dots & \dots & \dots & \dots & \dots \\ 0 & 0 & \dots & \mathbf{AN}^{m-1} & 0 \\ 0 & 0 & \dots & 0 & \mathbf{AN}^{m-1} \end{bmatrix}, \quad \boldsymbol{\alpha} = \begin{Bmatrix} \boldsymbol{\alpha}^1 \\ \dots \\ \boldsymbol{\alpha}^{n_q} \end{Bmatrix}, \quad \mathbf{H} = \begin{bmatrix} \operatorname{Re}(\mathbf{GN}_1) \cdot \mathbf{C}^{m-1} \\ \dots \\ \operatorname{Re}(\mathbf{GN}_{n_q}) \cdot \mathbf{C}^{m-1} \end{bmatrix}, \quad \mathbf{K} = \begin{bmatrix} -\operatorname{Im}(\mathbf{GN}_1) \cdot \mathbf{O}^{m-1} \\ \dots \\ -\operatorname{Im}(\mathbf{GN}_{n_q}) \cdot \mathbf{O}^{m-1} \end{bmatrix},$$

$$\mathbf{BN} = \begin{bmatrix} \mathbf{BN}^{m-1} & 0 & \dots & 0 & 0 \\ 0 & \mathbf{BN}^{m-1} & \dots & 0 & 0 \\ \dots & \dots & \dots & \dots & \dots \\ 0 & 0 & \dots & \mathbf{BN}^{m-1} & 0 \\ 0 & 0 & \dots & 0 & \mathbf{BN}^{m-1} \end{bmatrix}, \quad \boldsymbol{\beta} = \begin{Bmatrix} \boldsymbol{\beta}^1 \\ \dots \\ \boldsymbol{\beta}^{n_q} \end{Bmatrix}, \quad \mathbf{T} = \begin{bmatrix} \operatorname{Im}(\mathbf{GN}_1) \cdot \mathbf{C}^{m-1} \\ \dots \\ \operatorname{Im}(\mathbf{GN}_{n_q}) \cdot \mathbf{C}^{m-1} \end{bmatrix}, \quad \mathbf{S} = \begin{bmatrix} \operatorname{Re}(\mathbf{GN}_1) \cdot \mathbf{O}^{m-1} \\ \dots \\ \operatorname{Re}(\mathbf{GN}_{n_q}) \cdot \mathbf{O}^{m-1} \end{bmatrix},$$

$$\mathbf{b}_1 = \begin{Bmatrix} P_m^m \cdot \left[\operatorname{Re}(\mathbf{GN}_{11}) - \operatorname{mod}(m,2) \cdot \left(\operatorname{Re}(\mathbf{GN}_1) + \operatorname{Im}(\mathbf{GN}_1) \right) \right] \\ \dots \\ P_m^m \cdot \left[\operatorname{Re}(\mathbf{GN}_{n_q}) - \operatorname{mod}(m,2) \cdot \left(\operatorname{Re}(\mathbf{GN}_{n_q}) + \operatorname{Im}(\mathbf{GN}_{n_q}) \right) \right] \end{Bmatrix}$$

$$\mathbf{b}_2 = \begin{Bmatrix} P_m^m \cdot \left[\operatorname{Im}(\mathbf{GN}_1) + \operatorname{mod}(m,2) \cdot \left(\operatorname{Re}(\mathbf{GN}_1) - \operatorname{Im}(\mathbf{GN}_1) \right) \right] \\ \dots \\ P_m^m \cdot \left[\operatorname{Im}(\mathbf{GN}_{n_q}) + \operatorname{mod}(m,2) \cdot \left(\operatorname{Re}(\mathbf{GN}_{n_q}) - \operatorname{Im}(\mathbf{GN}_{n_q}) \right) \right] \end{Bmatrix} \tag{A.12}$$

Υ optimal least square functional can be defined:

$$\Upsilon(\boldsymbol{\alpha},\boldsymbol{\beta},\boldsymbol{\gamma},\boldsymbol{\mu})=\frac{1}{2}\left(\mathbf{e}_1^T\cdot\mathbf{e}_1+\mathbf{e}_2^T\cdot\mathbf{e}_2\right)\rightarrow\min \quad (A.13)$$

The stationary condition is applied to Υ, with respect to $\boldsymbol{\alpha}$. $\boldsymbol{\beta}$, $\boldsymbol{\gamma}$ and $\boldsymbol{\mu}$:

$$\begin{cases}\dfrac{\partial\Upsilon}{\partial\boldsymbol{\alpha}}=\mathbf{0}\\[4pt]\dfrac{\partial\Upsilon}{\partial\boldsymbol{\beta}}=\mathbf{0}\\[4pt]\dfrac{\partial\Upsilon}{\partial\boldsymbol{\gamma}}=\mathbf{0}\\[4pt]\dfrac{\partial\Upsilon}{\partial\boldsymbol{\mu}}=\mathbf{0}\end{cases}\Rightarrow\begin{cases}\mathbf{AN}^T\cdot\mathbf{AN}\cdot\boldsymbol{\alpha}=\mathbf{AN}^T\cdot\mathbf{H}\cdot\boldsymbol{\gamma}+\mathbf{AN}^T\cdot\mathbf{K}\cdot\boldsymbol{\delta}+\mathbf{AN}^T\cdot\mathbf{b}_1\\\mathbf{B}^T\cdot\mathbf{B}\cdot\boldsymbol{\alpha}=\mathbf{B}^T\cdot\mathbf{T}\cdot\boldsymbol{\gamma}+\mathbf{B}^T\cdot\mathbf{S}\cdot\boldsymbol{\delta}+\mathbf{B}^T\cdot\mathbf{b}_2\\\left(\mathbf{T}^T\mathbf{T}+\mathbf{H}^T\mathbf{H}\right)\cdot\boldsymbol{\gamma}-\mathbf{H}^T\cdot\mathbf{AN}\cdot\boldsymbol{\alpha}+\mathbf{H}^T\cdot\mathbf{K}\cdot\boldsymbol{\delta}+\mathbf{H}^T\cdot\mathbf{b}_1-\mathbf{T}^T\cdot\mathbf{B}\cdot\boldsymbol{\beta}+\mathbf{T}^T\cdot\mathbf{S}\cdot\boldsymbol{\delta}+\mathbf{T}^T\cdot\mathbf{b}_2=0\\\left(\mathbf{K}^T\mathbf{K}+\mathbf{S}^T\mathbf{S}\right)\cdot\boldsymbol{\mu}-\mathbf{K}^T\cdot\mathbf{AN}\cdot\boldsymbol{\alpha}+\mathbf{K}^T\cdot\mathbf{H}\cdot\boldsymbol{\delta}+\mathbf{K}^T\cdot\mathbf{b}_1-\mathbf{S}^T\cdot\mathbf{B}\cdot\boldsymbol{\beta}+\mathbf{S}^T\cdot\mathbf{T}\cdot\boldsymbol{\gamma}+\mathbf{S}^T\cdot\mathbf{b}_2=0\end{cases}\quad (A.14)$$

The $\left\{\boldsymbol{\alpha}^T\quad\boldsymbol{\beta}^T\quad\boldsymbol{\gamma}^T\quad\boldsymbol{\mu}^T\right\}^T$ solution can be obtained from Eq.(A.14):

$$\begin{cases}\boldsymbol{\gamma}\\\boldsymbol{\mu}\end{cases}=-\begin{bmatrix}\mathbf{H}^T\cdot\mathbf{AN}_0\cdot\mathbf{H}+\mathbf{T}^T\cdot\mathbf{BN}_0\cdot\mathbf{T}&\mathbf{H}^T\cdot\mathbf{AN}_0\cdot\mathbf{K}+\mathbf{T}^T\cdot\mathbf{BN}_0\cdot\mathbf{S}\\\mathbf{H}^T\cdot\mathbf{AN}_0\cdot\mathbf{K}+\mathbf{T}^T\cdot\mathbf{BN}_0\cdot\mathbf{S}&\mathbf{K}^T\cdot\mathbf{AN}_0\cdot\mathbf{K}+\mathbf{S}^T\cdot\mathbf{BN}_0\cdot\mathbf{S}\end{bmatrix}^{-1}\cdot\begin{bmatrix}\mathbf{H}^T\cdot\mathbf{AN}_0&\mathbf{T}^T\cdot\mathbf{BN}_0\\\mathbf{K}^T\cdot\mathbf{AN}_0&\mathbf{S}^T\cdot\mathbf{BN}_0\end{bmatrix}\cdot\begin{Bmatrix}\mathbf{b}_1\\\mathbf{b}_2\end{Bmatrix}$$

$$\begin{cases}\boldsymbol{\alpha}=\left(\mathbf{AN}^T\cdot\mathbf{AN}\right)^{-1}\cdot\mathbf{AN}\cdot\begin{bmatrix}\mathbf{H}&\mathbf{K}&\mathbf{I}\end{bmatrix}\cdot\begin{bmatrix}\boldsymbol{\gamma}&\boldsymbol{\mu}&\mathbf{b}_1\end{bmatrix}^T\\\boldsymbol{\beta}=\left(\mathbf{BN}^T\cdot\mathbf{BN}\right)^{-1}\cdot\mathbf{BN}\cdot\begin{bmatrix}\mathbf{T}&\mathbf{S}&\mathbf{I}\end{bmatrix}\cdot\begin{bmatrix}\boldsymbol{\gamma}&\boldsymbol{\mu}&\mathbf{b}_2\end{bmatrix}^T\end{cases}\quad (A.15)$$

$$\mathbf{AN}_0=\mathbf{I}-\mathbf{AN}\cdot\left(\mathbf{AN}^T\cdot\mathbf{AN}\right)^{-1}\cdot\mathbf{AN}^T\quad,\quad\mathbf{BN}_0=\mathbf{I}-\mathbf{BN}\cdot\left(\mathbf{BN}^T\cdot\mathbf{BN}\right)^{-1}\cdot\mathbf{BN}^T$$

From Eq.(A.15) the rational fit parameters can be obtained. The physically sound optimal m model order can be found by eliminating unphysical (poles with positive real part or complex conjugate pole couples associated to natural frequency external to the frequency excitation range) and unstable poles and their residues, where pole stability is evaluated by means of stability diagrams [12]. The contribution of discarded pole-residue couples is taken into account by adding a third-grade polynomial function to the identified rational function [4,12].

Declaration of Competing Interest

The authors declare that they have no known competing financial interests or personal relationships that could have appeared to influence the work reported in this paper.

CRedit authorship contribution statement

References:

[1] Read BE, Dean G D. The Determination of Dynamic Properties of Polymers and Composites. Adam Hilger Ltd, Bristol, England, 1978.

[2] Ehrenstein GW, Trawiel P, Riedel G. Thermal Analysis of Plastics Theory and Practice. Carl Hanser Verlag GmbH & Co. KG, 2004.

[3] Menard KP. Dynamic Mechanical Analysis: A practical Introduction Second Edition. CRC Press 2008.

[4] Amadori S, Catania G. Robust identification of the mechanical properties of viscoelastic non-standard materials by means of frequency domain experimental measurements. Composite Structures 2017; 169: 79 – 89.

[5] D5023-07: Standard Test Method for Plastics: Dynamic Mechanical Properties: In Flexure (Three-Point Bending), ASTM International (2015).

[6] D5418-15: Standard Test Method for Plastics: Dynamic Mechanical Properties: In Flexure (Dual Cantilever Beam), ASTM International (2015).

[7] Placet V, Foltete E. Is Dynamic Mechanical Analysis (DMA) a non-resonance technique? EPJ Web of Conference (41004) 2010.

[8] Danley RL. Dynamic mechanical analyzer and sample fixture for dynamic mechanical analyzer. U.S. Patent 9,933,249 filed Decemberr 4, 2014, and issued April 3, 2018.

[9] Storage T., Brockman R, Tienda KM. Analysis of Data Reduction Strategy used in TA Instruments Q800 DMA Test System. 2013 Available online: https://apps.dtic.mil/dtic/tr/fulltext/u2/a591605.pdf.

[10] McAninch IM, Palmese GR, Lenhart JL, La Scala JJ. DMA testing of epoxy resins: The importance of dimensions. Polym Eng Sci 2015, 55: 2761-2774.

[11] Schalnat J, Garoz Gómez D, Daelemans L, De Baere I, De Clerck K, Van Paepegem W. Influencing parameters on measurement accuracy in dynamic mechanical analysis of thermoplastic polymers and their composites. Polymer Testing 2020, vol .91.

[12] Ewins DJ. Modal testing: theory, practice and applications. Research Studies Press, 2000.

[13] Peumans D, De Vestel A, Busschots c, Rolain Y, Pintelon R, Vandersteen G. Accurate estimation of the non-parametric FRF of lightly-damped mechanical systems using arbitrary excitations. Mechanical Systems and Signal Processing, 2019, 130: 545-564.

[14] Huynh HN, Assadi H, Dambly V, Lorphèvre ER, Verlinden O. Direct method for updating flexible multibody systems applied to a milling robot. Robotics and Computer-Integrated Manufacturing 2021, 68: 102049.

[15] Warren C, Niezrecki C, Avitabile P, Pingle P. Comparison of FRF measurements and mode shapes determined using optically image based, laser, and accelerometer measurements. Mechanical Systems and Signal Processing 2011, 25(6): 2191-2202.

[16] Huynh HN, Assadi H, Lorphèvre ER, Verlinden O, Ahmadi K. Modelling the dynamics of industrial robots for milling operations. Robotics and Computer-Integrated Manufacturing 2020, 61: 101852.

[17] Richardson MH, Formenti DL. Parameter Estimation From Frequency Response Measurements Using Rational Fraction Polynomials. In Proceedings of 1st IMAC Conference, Orlando, FL, 1982.

[18] Timoshenko S, Young DH, Weaver Jr W. Vibration Problems in Engineering John Wiley & Sons Inc., 1974.

[19] Findley WN, Lai JS, Onaran K. Creep and Relaxation of Nonlinear Viscoelastic Materials. New York: Dover publications Inc., 1989.

[20] Forsythe GE. Journal of the Society of Industrial Applied Mathematics. 1957;5(2): 74-85.

[21] Kelly LG. Handbook of Numerical Methods and Applications. Addison Wesley Publishing Company, 1967.

[22] Forsythe GE, Malcolm MA, Moler CB. Computer Methods for Mathematical Computations. Prentice-Hall Englewood Cliffs NJ, 1977

[23] Allemang RJ, Phillips AW. The Unified Matrix Polynomial Approach to Understanding Modal Parameter Estimation: An Update. In Proceedings of the 2004 International Conference on Noise and Vibration Engineering, ISMA, Leuven, Belgium, 2004, p. 2373-2408.

[24] Catania G; Zanarini A. Flexible Multibody System Dynamics by Means of a Spectral Based Meshless Approach. Advances In Applied Mathematics and Mechanics 2019, 11: 757 - 806)

[25] Gill PE, Murray W, Wright MH. Practical Optimization. London, Academic Press, 1981

[26] Coleman TF, Li Y. An Interior, Trust Region Approach for Nonlinear Minimization Subject to Bounds. SIAM Journal on Optimization, 1996;6:418–445.

[27] Abramson MA. Pattern Search Filter Algorithms for Mixed Variable General Constrained Optimization Problems. Ph.D. Thesis, Department of Computational and Applied Mathematics, Rice University, August 2002.

[28] Kolda TG, Torzcon VJ, Lewis RM. A generating set direct search augmented Lagrangian algorithm for optimization with a combination of general and linear constraints. Technical Report SAND2006-5315, Sandia National Laboratories, August 2006.